Continental weathering as a driver of Late Cretaceous cooling: new insights from clay mineralogy of Campanian sediments from the southern Tethyan margin to the Boreal realm

Chenot Elise (1), Deconinck Jean-François (1), Pucéat Emmanuelle (1), Pellenard Pierre (1), Guiraud Michel (1), Jaubert Maxime (1), Jarvis Ian (2), Thibault Nicolas (3), Cocquerez Théophile (1), Bruneau Ludovic (1), Razmjooei Mohammad J. (4), Boussaha Myriam (3), Richard James (5), Sizun Jean-Pierre (5), Stemmerik Lars (6)

(1) Biogéosciences, UMR 6282, UBFC/CNRS, Univ. Bourgogne Franche-Comté, 6 boulevard Gabriel, F-21000 Dijon, France.

(2) Department of Geography and Geology, Kingston University London, Penrhyn Road, Kingston upon Thames KT1 2EE, United Kingdom.

(3) IGN, University of Copenhagen, Øster Voldgade 10, DK-1350 Copenhagen, Denmark.

(4) Department of Geology, Faculty of Earth Science, Shahid Beheshti University, Tehran, Iran.

(5) Chrono-environnement, UMR 6249 UBFC/CNRS, Univ. Bourgogne Franche-Comté, 16 route de Gray, F-25030 Besançon, France.

(6) Natural History Museum, University of Copenhagen, Øster Voldgade 5-7, DK-1350 Copenhagen, Denmark.

Abstract

New clay mineralogical analyses have been performed on Campanian sediments from the Tethyan and Boreal realms along a palaeolatitudinal transect from 45° to 20°N (Danish Basin, North Sea, Paris Basin, Mons Basin, Aquitaine Basin, Umbria-Marche Basin and

Tunisian Atlas). Significant terrigenous inputs are evidenced by increasing proportions of detrital clay minerals such as illite, kaolinite and chlorite at various levels in the mid- to upper Campanian, while smectitic minerals predominate and represented the background of the Late Cretaceous clay sedimentation. Our new results highlight a distinct latitudinal distribution of clay minerals, with the occurrence of kaolinite in southern sections and an almost total absence of this mineral in northern areas. This latitudinal trend points to an at least partial climatic control on clay mineral sedimentation, with a humid zone developed between 20° and 35°N. The association and co-evolution of illite, chlorite and kaolinite in most sections suggest a reworking of these minerals from basement rocks weathered by hydrolysis, which we link to the formation of relief around the Tethys due to compression associated with incipient Tethyan closure. Diachronism in the occurrence of detrital minerals between sections, with detrital input starting earlier during the Santonian in the south than in the north, highlights the northward progression of the deformation related to the anticlockwise rotation of Africa. Increasing continental weathering and erosion, evidenced by our clay mineralogical data through the Campanian, may have resulted in enhanced CO_2 consumption by silicate weathering, thereby contributing to Late Cretaceous climatic cooling.

Keywords: Campanian, Late Cretaceous cooling, clay minerals, carbon isotope stratigraphy, climatic belt, continental weathering

1. Introduction

The Late Cretaceous is characterised by a long-term global climatic cooling from the Turonian onward, with a marked acceleration during the Campanian (Huber et al., 1995; Pucéat et al., 2003; Friedrich et al., 2012; Linnert et al., 2014). This period shows evidence of

an overall decrease in atmospheric CO_2 levels that likely contributed to this global cooling, although the data remain scarce and do not allow to identify the timing and phases of CO_2 decline within the Late Cretaceous (Royer et al., 2012; Wang et al., 2014; Franks et al., 2014). Decreasing mantle degassing linked to variations in seafloor production rates and continental arc magmatism has been invoked to explain the observed decline in CO_2 levels during the Late Cretaceous (Berner, 2004; Cogné and Hummler, 2006; Van Der Meer et al., 2014; McKenzie et al., 2016).

Continental silicate weathering also governs atmospheric CO_2 on a multi-million year time scale (Berner, 1990, 2004; Raymo and Ruddiman 1992; Dessert et al., 2003), but this process remains poorly explored for the Late Cretaceous. Yet this period was marked by major geodynamic changes, which included the initiation of Tethys Ocean closure (Dercourt et al., 1986). This event, which is linked to the convergence of Africa toward Eurasia, was associated with the development of topographic relief around the Tethys, including lithospheric folds in Morocco (Frizon de Lamotte et al., 2011), and the 5000 km long chain of relief developed across North Africa and the Middle East by the Ayyubid orogeny (Şengör and Stock, 2014). This increased relief might be expected to have induced an increase in continental silicate weathering, enhancing CO_2 consumption.

Clay minerals assemblages may be used to assess fluctuations in continental weathering intensity (Chamley, 1989; Hermoso and Pellenard, 2014). Numerous clay minerals data exist for the Cenomanian, Turonian and Maastrichtian stages but they remain scarce for the Santonian–Campanian interval although many significant environmental changes occurred at that time. A major reorganization of oceanic circulation took place during the Santonian–Campanian, evidenced by neodymium isotope data (Robinson et al., 2010; Martin et al., 2012; Moiroud et al., 2016). The Campanian stage was also characterised by a

75 significant cooling, as indicated by $\delta^{18}O$ values of benthic foraminifera and TEX_{86} data
76 (Friedrich et al., 2012; Linnert et al., 2014; O'Brien et al., 2017).

77 At a regional scale, preliminary clay minerals data from the Tercis-les-Bains section
78 (Aquitaine basin, North Atlantic influenced) and from the Poigny borehole (Paris basin,
79 Boreal influenced) have shown increasing inputs of detrital illite and kaolinite during the
80 Campanian (Chenot et al., 2016), coinciding with a global carbon-isotope negative excursion,
81 the so-called "Late Campanian Event" of Jarvis et al. (2002). This suggests that changes in the
82 carbon cycle at this time were accompanied by an increase of continental weathering. In order
83 to explore the spatial and temporal extent of these modifications in continental weathering, we
84 have acquired new data for clay minerals assemblages from Campanian sediments through 6
85 different sections and boreholes from the Tethyan and Boreal realms, along a transect from
86 ~18° to ~42°N palaeolatitude. Combined with previously published data sets, our work
87 provides the first constrains at the Tethyan scale on variations in continental weathering
88 induced by tectonic uplift during the Campanian.
89
90 2. Geodynamic framework and global palaeogeography of the studied sites
91
92 From the mid-Cretaceous onward, global plate tectonic changes induced modification of
93 the tectonic stress field in Europe. The Tethys Ocean began to close due to the anticlockwise
94 movement of Africa, with: (1) at the northern margin, the opening of the Bay of Biscay and
95 active subduction zones in Apulia, the Dinarides and Hellenids; and (2) at the southern
96 margin, the development of an intra-oceanic orogenic belt (Smith, 1971; Dewey et al., 1973;
97 Charvet, 1978; Bárdossy and Dercourt., 1990; Faccenna et al., 2001; Blakey, 2008; Kley and
98 Voigt, 2008; Voigt et al., 2008; Fig. 1).

To the north, the interplay of extensional and compressional tectonics, resulting from the west-central Europe's thin lithosphere pinch between Baltica's and Africa's cratonic lithospheres, induced NW–SE striking thrust faulting on the European plate (Kley and Voigt, 2008). These processes caused the development of subsiding basins (e.g. Sorgenfrei-Tornquist Zone), and inversions of former depocentres (e.g. Mid-Polish Trough), with different rates of subsidence (Kley and Voigt, 2008; Voigt et al., 2008). These newly created reliefs provided detrital particles into the adjacent seas (Fig. 1). The geology of the southern margin of Central Europe resulted from the convergence linked to the subduction zone between the European and African plates.

Campanian palaeogeographic reconstructions show that the northern Tethyan margin was partly covered by epicontinental seas (Fig. 1), with emerged lands representing remnants of Variscan relief (e.g. Armorican, Central, Iberian, Ebro, Welsh, Rhenish, Bohemian massifs), the inverted Mid-Polish Anticline (Voigt et al., 2008), and regional shoals (Dalmatian shoal, High Karst; Charvet, 1978). The southern passive continental margin of the Tethys Ocean was a wide platform (e.g. Saharan platform, Syrte basin), influenced by several detrital sources, including locally emerged land masses such as Kasserine Island in Tunisia (Kadri et al., 2015) and the north-western African craton (Fig. 1). However, the palaeogeography of Central Europe is more difficult to reconstruct because of the large area affected by erosion during the Late Cretaceous inversion (Voigt et al., 2008; Wolfgring et al., 2016; Neuhuber et al., 2016).

2.1. Boreal Realm

2.1.1. Danish North Sea and eastern Danish basin: Stevns-2 and Adda-3 boreholes

123 The Chalk Group of the Danish North Sea is well studied for its hydrocarbons reservoir
124 properties (Hardman, 1982; Megson and Tygesen, 2005). During the Late Cretaceous, the
125 Danish basin was bordered by the Baltic Shield to the northeast, the Grampian High to the
126 northwest, and the Rhenish–Bohemian Massif to the south (Fig. 1).
127 The 350 m long Stevns-2 core was drilled in Boesdal Quarry (55°15'31''N 12°24'04''E)
128 located in the eastern part of the Danish basin (palaeolatitude ~42°N; Philip and Floquet,
129 2000; Fig. 1). The core recovers a complete succession of upper Campanian to Maastrichtian
130 chalks, with a distinctive interval of alternating chalk-marl in the upper Campanian, a feature
131 that is also observed in the nearby Stevns-1 core and appears to characterise the whole Stevns
132 peninsula (Thibault et al., 2016a). The calcareous nannofossils biostratigraphy, high-
133 resolution carbon- and oxygen-isotope chemostratigraphy, and sedimentology of the Stevns-2
134 core have been described by Boussaha et al. (2016, 2017; Fig. 2).
135 The Adda-3 well in the Danish Central Graben (55°47'50"N 04°53'26"E) is located in the
136 southern part of the North Sea rift system (palaeolatitude ~45°N; Philip and Floquet, 2000;
137 Fig. 1). The Campanian interval, composed of bioturbated white chalks with occasional thick
138 flint bands and marly layers, occurs between 2200.8–2260.8 m depth. The calcareous
139 nannofossils biostratigraphy and stable-isotope geochemistry ($\delta^{13}C$, $\delta^{18}O$) have been
140 presented by Perdiou et al. (2016; Fig. 2).
141
142 2.1.2. Mons Basin: Cbr-7 borehole
143
144 The Mons basin (southern Belgium) was a transitional area between the North Sea and the
145 Paris basin to the WSW, bordered by the Rhenish Massif to the ENE (palaeolatitude ~37°N;
146 Philip and Floquet, 2000; Fig. 1). Based on lithology, the Campanian chalk of the Mons basin
147 has been subdivided into three formations (Cornet and Briart, 1870; Briart and Cornet, 1880):

148 the Trivières Chalk (white to grey marly chalk without flint); the Obourg Chalk (fine white
149 chalk with flint in the north of the Mons basin); and the Nouvelles Chalk (fine white chalk
150 without flint).

151 The 75 m-deep Cbr-7 borehole was drilled on the northern margin of the Hainaut-Sambre
152 quarry (50°25'10"N 04°1'33"E) located in the southeast of the Mons basin (Fig. 1).
153 Robaszynski and Anciaux (1976) subdivided the succession into the: Trivières Chalk (75.0–
154 46.5 m depth); Obourg Chalk (46.5–30.5 m); and Nouvelles Chalk (30.5–2.4 m depth).
155 Biostratigraphic data are scarce, but the uppermost part of the Trivières Chalk, the Obourg
156 Chalk and Nouvelles Chalk have been attributed to the lower part of the upper Campanian
157 according to the vertical distribution of foraminifera, belemnites and echinoids (Robaszynski
158 and Christensen, 1989; Fig. 3). A hardground exhibiting high Mn concentrations, acquired by
159 inductively coupled plasma-atomic emission spectrometry (ICP-AES) in the original study of
160 Richard et al. (2005) and an important $\delta^{13}C$ negative excursion of 0.5‰ amplitude occurs in
161 the uppermost part of the Trivières Chalk.
162
163 2.2. Tethyan Realm
164
165 2.2.1. Umbria-Marche basin: Gubbio – la Bottaccione and Furlo – Upper Road sections
166
167 A thick succession of Upper Cretaceous pelagic carbonates was deposited in the Umbria-
168 Marche basin in central Italy. During the Late Cretaceous, this deep basin was surrounded by
169 the High-Karst to the northeast (Charvet, 1978; palaeolatitude ~25°N; Philip and Floquet,
170 2000; Fig. 1). The symmetric NE–SW anticline of the Gubbio – la Bottaccione section
171 (43°21'45"N 12°34'57"E; Fig. 1) exposes a succession of pelagic carbonates from the Upper
172 Jurassic to the Palaeocene (~400 m-thick), followed by the first terrigenous turbidites within

the Miocene (Arthur and Fisher, 1977). The Campanian–Maastrichtian Scaglia Rossa Formation is composed of pelagic carbonates with small quantities of iron oxides, including magnetite and hematite, responsible for the pink colour of the limestones (Lowrie and Alvarez, 1977; Channell et al., 1982; Lowrie and Heller, 1982).

The Campanian Scaglia Rossa Formation of Gubbio – la Bottacione shows many prominent 5 to 10 cm-thick cherty beds in the lower Campanian, overlain by a 5 m-thick marly interval (Fig. 4). Many stratigraphic studies, including pioneering magnetostratigraphy (Lowrie and Alvarez, 1977) and biostratigraphy based on foraminifera (Premoli Silva, 1977), have been published for the section. In this paper we use the stratigraphic data from Coccioni and Premoli Silva (2015) who recently revised the Upper Albian–Maastrichtian bio- and magnetostratigraphy of this Tethyan reference section.

The Furlo – Upper Road section (43°38'29"N 12°42'36"E) located north of the Umbria-Marche basin (Fig. 1) exposes pelagic carbonate deposits from the Jurassic to the Palaeocene (~300 m-thick). A well-defined magnetostratigraphy (Alvarez and Lowrie, 1984) and a U/Pb age from a bentonite layer identified within chron C33r (Mattias et al., 1988; Bernoulli et al., 2004), provide a stratigraphic framework for the Campanian–Maastrichtian interval. Slope deposits are expressed in the upper part of the section by the occurrence of more than 70 (10 to 100 cm-thick) white-coloured turbidites, and by a 12 m-thick slump at the base of chron C33n (Fig. 4).

2.2.2. Tunisian Atlas: El Kef – El Djebil section

During the Campanian–Maastrichtian, the Saharan platform was located at ~18°N on the southern margin of the Tethys Ocean (Philip and Floquet, 2000; Fig. 1). The closure of the Tethys generated tectonic compressive and extensive domains; the Saharan platform belonged

198 to an external domain of intracontinental deformation, far from the intra-oceanic deformation
199 zone to the north (Aris et al., 1998; Boutib et al., 2000; Frizon de Lamotte et al., 2009; Bey et
200 al., 2012).

201 The 500-m thick El Kef – El Djebil section, located in the Tunisian Atlas immediately to
202 the north of the Saharan platform (36°10'37"N 08°44'05"E) corresponds to the Abiod Chalk
203 Formation. The Campanian–Maastrichtian Abiod Formation comprises three members
204 (Burollet, 1956; Jarvis et al., 2002; Fig. 3), from base to summit: white chalks with occasional
205 calciturbidites (lower chalk 'bar' or Haraoua Member); bioturbated marls with common
206 limestone beds (middle marl or Akhdar Member); and a yellow-greyish bioturbated chalky
207 unit (upper chalk 'bar' or Ncham Member). The biostratigraphic framework is mainly based
208 on well-preserved planktonic foraminifers, complemented by carbon isotope
209 chemostratigraphy (Robaszynski et al., 2000; Jarvis et al., 2002; Mabrouk El Asmi, 2014).
210
211 ## 3. Materials and Methods
212
213 ### 3.1. Oxygen and carbon isotopes
214
215 New stable-isotope data were generated for the two Italian studied sections
216 (Supplementary Data A, B). Wherever possible, samples were recovered for geochemical
217 analyses every metre from the Gubbio – la Bottaccione section and every half metre from the
218 Furlo – Upper Road section. Stable-isotope analyses of carbonate ($\delta^{13}C_{carb}$ and $\delta^{18}O_{carb}$) were
219 performed on bulk rocks collected along the whole of each section, from the Santonian–
220 Campanian boundary to the Campanian–Maastrichtian boundary (Fig 4). Isotopic analyses
221 were carried out at the Leibniz–Laboratory für Altersbestimmung und Isotopenforschung,
222 Christian–Albrechts University, Kiel, Germany. Samples devoid of macrofossils were crushed

in an agate mortar and pestle into fine and homogeneous calcite powders, which were reacted with 100% phosphoric acid at 70°C and analysed using a ThermoScientific MAT253 mass spectrometer, connected to a Kiel IV preparation device. Eleven samples from the Gubbio – la Bottaccione section were additionally analysed at the Biogéosciences Laboratory, University of Bourgogne Franche-Comté, Dijon, France. Here, calcite was reacted with 100% phosphoric acid at 90°C using a Multiprep online carbonate preparation line connected to an Isoprime mass spectrometer.

All isotopic values are reported in the standard δ-notation in per mil relative to V-PDB (Vienna Pee Dee Belemnite) by assigning a $\delta^{13}C$ value of +1.95‰ and a $\delta^{18}O$ value of −2.20‰ to NBS19. External reproducibility as determined by replicate analyses of laboratory standards was ±0.08‰ (2σ) for oxygen isotopes in both laboratories and ±0.05‰ (2σ) for carbon isotopes at Leibniz – Laboratory and ±0.04‰ at the Biogéosciences Laboratory.

3.2. Clay mineralogy

All bulk-rock samples were collected in the field and from the core storage facility with a regular sample spacing (Figs 2–4). Mineralogical analyses were performed at the Biogéosciences Laboratory, University of Bourgogne Franche-Comté. Clay minerals assemblages were identified by X-ray diffraction (XRD) on oriented mounts of non-calcareous clay-sized particles (<2 μm). The procedure described by Moore and Reynolds (2009) was used to prepare all samples to better compare the integrity of the dataset and to avoid discrepancies due to the process of quantification. Diffractograms were obtained using a Bruker D4 Endeavor diffractometer employing CuK_{α} radiation with a LynxEye detector and Ni filter, under 40 kV voltage and 25 mA intensity. For each sample, three preparations were

247 analysed: after air-drying; after ethylene-glycol solvation; and after heating at 490°C for 2
248 hours. The goniometer was scanned from 2.5° to 28.5° 2θ for each run.

249 Clay minerals were identified by the positions of their main diffraction peaks on the
250 three XRD runs (Table 1), while semi-quantitative estimates were produced in relation to their
251 peak areas (Moore and Reynolds, 2009). Peak areas were determined on diffractograms of
252 glycolated runs with MacDiff 4.2.5 software (Petschick, 2010). The percentages of kaolinite
253 and chlorite were determined by deconvolution of the $d(002)_{kaolinite}$ and $d(004)_{chlorite}$ peak
254 areas that appear respectively at 3.57 and 3.52Å and using the 7.1Å peak area common to
255 both minerals. Beyond the evaluation of the absolute proportions of the clay minerals, the aim
256 was to identify their relative fluctuations through the sections.

257 Measurement of the relative proportions of smectite and illite layers in the R0 mixed
258 layers were performed on the diffractograms, following two methods: the procedure of Moore
259 and Reynolds (2009) and the determination of the saddle Index after Inoue et al. (1989). In
260 most cases, the procedure of Moore and Reynolds was performed on reflections 001/002 and
261 002/003. However, the presence of illite at 10Å stretches the 001/002 reflection and modifies
262 the true position of 001/002. In this case, estimation of the smectite layers was determined
263 only using the reflection 002/003.

264

265 3.3. Correlation of the studied sites: $\delta^{13}C_{carb}$ isotopic events

266

267 We have used global and local carbon-isotope events previously recognised in the
268 Campanian to correlate sections and boreholes. During the Campanian, seven isotopic events
269 have been identified.

270 - The Santonian–Campanian Boundary Event (SCBE), consisting of a global positive
271 shift of $\delta^{13}C_{carb}$, with a varying amplitude of 0.3‰ to 2.9‰ (Jarvis et al., 2002; Gale et

al., 2008; Wendler, 2013; Thibault et al., 2016b; Dubicka et al., 2017), has been widely recognised in successions throughout the Boreal, Tethyan, North Pacific and Central Atlantic realms (Table 2, Event 1). This event coincides with the C34/C33r chron boundary and the Highest Occurrence (HO) of the crinoid *Marsupites testudinarius*, both defining the Santonian–Campanian boundary (Italy, Gubbio – la Bottaccione, Premoli Silva and Sliter, 1994; Texas, Waxahachie Dam Spillway, Gale et al., 2008; Poland Bocieniec, Dubicka et al., 2017).

- The *papillosa* Zone Event (PZE) is a positive excursion of ~0.2‰ coincident with a medium-term $\delta^{13}C$ maximum, occurring in the mid-Lower Campanian *papillosa* zone at Lägerdorf and in the uppermost *Globotruncana elevata* zone (Chron 33r/33n boundary) on the Bottaccione section. Its stratigraphic significance still needs to be tested by additional high-resolution data sets (Thibault et al., 2016b; Sabatino et al., 2018; Table 2, Event 2).
- The Mid-Campanian Event (MCE), first described by Jarvis et al. (2002) on the $\delta^{13}C_{carb}$ curves of El Kef (Tethyan realm, Tunisia), Bidart (North Atlantic realm, France) and Trunch (Boreal realm, England, Jenkyns et al., 1994), is defined by a positive excursion of 0.3‰ occurring near the base of *Globotruncana ventricosa* planktonic foraminifera zone and the base of the upper Campanian (Table 2, Event 3). At Tercis-les-Bains, this event occurs at the base of chron C33n, comprising the Lowest Occurrence (LO) of *Rucinolithus magnus* and *Uniplanarius gothicus* nannofossils. This event has been recognised at a larger scale by Perdiou et al. (2016) in the North Sea.
- The Conica Event (CE; Perdiou et al., 2016) is a small negative excursion of $\delta^{13}C_{carb}$ of ~0.4‰, occurring at the base of the *conica-senior* macrofossil zone, in the Boreal and North Atlantic realms (Table 2, Event 4).

- The Late Campanian Event (LCE) is a global event, identified in the Tethyan, Boreal, Central Pacific, Indian Ocean and North Atlantic realms (Jarvis et al., 2002, 2006; Voigt et al., 2010, 2012; Thibault et al., 2012b; Sabatino et al., 2018). It consists of a marked negative excursion of $\delta^{13}C_{carb}$ with an amplitude varying between 0.3‰ and 1.3‰. It is located within the middle of chron C33n (Table 2, Event 5). This event occurs within (Gubbio, Voigt et al., 2012; Sabatino et al., 2018) and/or immediately above (El Kef, Jarvis et al., 2002; Tercis-les-Bains, Voigt et al., 2012, Chenot et al., 2016) the *Radotruncana calcarata* planktonic foraminifera zone (UC15 d-e nannofossil zone) in the Tethyan realm and in the mid-*Belemnitella mucronata* macrofossil zone in the Boreal realm. Perdiou et al. (2016) identified two steps in this isotopic event, called the pre-LCE and the main-LCE, which coincide with an increase of illite, kaolinite and chlorite in the Aquitaine basin (Chenot et al., 2016) and illite in the Paris basin (Deconinck et al., 2005).
- The Epsilon event (EE or C1-) was defined by Thibault et al. (2012a) as a negative excursion of ~0.25‰, followed by a positive shift of 0.2‰ and a second negative excursion of 0.1‰, which imparts to this event a sharp resemblance to the Greek letter ε. The event occurs slightly above the HO of *Eiffellithus eximius* in the Boreal, Tethyan and North Atlantic realms (Table 2, Event 6).
- The Campanian–Maastrichtian Boundary Event (CMBE, Voigt et al., 2010, 2012) is a global negative event with an amplitude ranging from 0.3‰ to 1‰, occurring in the reverse chron C32n2n, and identified in many sedimentary basins from the Tethyan to Pacific realms (Table 2, Event 7). This isotopic event was divided into three steps by Thibault et al. (2012a): CMBa (negative excursion of 0.6‰); CMBb (positive excursion of 0.2‰); CMBc (negative excursion of 0.4‰). The definition of the CMBE by Voigt et al. (2012) is different as it comprises the whole long-term decrease

in carbon isotopes ranging from the middle of chron C32n2n up to the lower half of chron C31r and is further described by 5 distinct small positive peaks that are superimposed on the long-term trend (CMBE1 to CMBE5).

3.4. Calcareous nannofossils biostratigraphy

The El Kef – El Djebil section constitutes one of the reference isotopic curves for the Campanian of the Tethys (Jarvis et al., 2002) but so far, no calcareous nannofossils biostratigraphy was available for that section. In this study, we analysed 17 samples from the archive of Jarvis et al. (2002) in order to establish a coarse calcareous nannofossils biostratigraphy that can be directly correlated to the already available isotope curve. Standard smear-slides were prepared following the methodology described in Bown (1998) and the biostratigraphy is based solely on presence/absence of individual taxa observed in crossed nicols at a magnification of x1000 on a Leica DM750P optical microscope. The CC nannofossil zonation of Sissingh (1977) modified by Perch-Nielsen (1985) and the UC^{TP} (Tethyan Province) zonation of Burnett (1998) have been applied (Fig. 5).

3.5. Calcium carbonate content

Calcimetry was performed on the Gubbio – la Bottaccione and Cbr-7 samples at the Biogéosciences Laboratory, University of Bourgogne Franche-Comté, using a Bernard calcimeter. The samples were treated with hydrochloric acid and the CO_2 released was used to quantifying the percentage of $CaCO_3$. The data are reported on Fig. 3 and Supplementary Data C for the Cbr-7 borehole and in Supplementary Data B for the Gubbio – la Bottaccione section.

4. Results

4.1. Clay mineralogy

The clay fraction of the six studied sites is composed predominantly (often more than 80%) of R0 random illite/smectite mixed-layers; hereafter referred to as smectitic minerals (not represented on Figs. 2–4 to emphasize other clay minerals variations; Supplementary Data A, B; C, D, E, F). This result was expected, since Upper Cretaceous sediments are characterised by an abundance of these minerals, considered to be the background of the clay sedimentation (Deconinck and Chamley, 1995; Deconinck et al., 2005; Jeans, 2006; Chenot et al., 2016). Other clay minerals, occurring in significant proportions, include illite, chlorite, kaolinite and palygorskite.

4.1.1. Stevns-2 and Adda-3 boreholes

Illite (less than 10% of the clay fraction) occurs in most samples from the Stevns-2 borehole. Traces of chlorite (less than 2%) are recorded between 349.9 and 251.7 m depth corresponding to beds of alternating chalk-marl and higher gamma-ray values of the upper Campanian; this interval is associated with a warm optimum preceding the early Maastrichtian cooling (Thibault et al., 2016a; Boussaha et al., 2017). Chlorite is absent above the Campanian–Maastrichtian boundary (Fig. 2; Supplementary Data D). The clay minerals assemblage of the Adda-3 borehole includes traces of illite and traces of kaolinite in all samples (Fig. 2; Supplementary Data E). Based on the methods of Moore and Reynolds (2009) and Inoue et al. (1989), estimation of the smectite layers in the IS R0 comprises

between 50 and 80% in the Stevns-2 borehole (Supplementary Data D) and between 85 and 95% in the Adda-3 borehole (Supplementary Data E). The evolution of the percentage does not show any trend.

4.1.2. Cbr-7 borehole

According calcium carbonate content data, the percentage of the clay fraction is estimated to range between 5% from 75 to ~40 m depth to < 3% from ~40 m to the top of the core (Fig. 3; Supplementary Data C).

In the Trivières Chalk, at the base of the core, beside smectitic minerals, the clay assemblages consist of 20% illite, with small quantities of kaolinite that decrease from the base to the top of the formation (from less than 10% to traces). Kaolinite disappears in the overlying Obourg Chalk, while illite occurs in small proportions in this formation, together with traces of fibrous clays (palygorskite), clinoptilolite and talc. The Nouvelles Chalk is characterised by increasing proportions of illite with varying quantities of fibrous clays, clinoptilolite and talc (Fig. 3).

To estimate the percentage of smectite layers in the IS R0, the method of Moore and Reynolds (2009) could not be performed on the Cbr-7 borehole diffractograms because reflections 001/002 and 002/003 are poorly expressed. However, the method of Inoue et al. (1989) shows an evolution of the Saddle Index similar to the trend of illite. First, from 80 to 45 m depth, the saddle index displays a decreasing trend from 0.7 to 0.3, which means an increase of smectite layers in the IS R0 (from ~60 to ~80%). In a second part, the saddle index records an increasing trend between 45 – 10 m depth from 0.3 to 1, interrupted by highest values around 35 m, corresponding to smectite layers ranging from ~80 to ~50%. At the top

of the borehole, from 7 to 3 m depth, the saddle index displays the lowest values around 0.5, equivalent to about 70% of smectite layers (Supplementary Data C).

4.1.3. Gubbio – la Bottaccione and Furlo – Upper Road sections

In the Gubbio – la Bottaccione section, from the base to 45 m, beside abundant smectitic minerals, the clay fraction consists of illite (10%) with occasional traces of kaolinite and chlorite (Fig. 4; Supplementary Data B), while from 50 to 70 m, kaolinite and chlorite occur systematically and increase up to maxima of >5% along with abundant illite (50%). In the uppermost part of the section, the proportions of kaolinite and chlorite decrease and kaolinite essentially disappears from 80 m upwards. From the base to 50 m, the percentage of smectite layers in the IS R0 is estimated to ~70%, whereas from 50 to 80 m, it decreases until ~50%. From 80 m to the top of the section, smectite layers increase again to ~65 % (Supplementary Data B).

From the base of the Furlo section to 44 m, the percentage of illite is around 10% with traces of kaolinite (Fig. 4; Supplementary Data A). From 57 m, kaolinite increases significantly, rising upwards to >10% at 75 m, together with more abundant illite and traces of chlorite. Interestingly, the onset of this major mineralogical change coincides with the appearance of turbidites above a 12 m-thick slump. The percentage of smectite layers in the IS R0 follows an opposite trend compared to illite until 80 m: from the base of the section to 44 m the highest percentage of smectite layers is estimated to ~70% and then progressively decreases down to ~50%. However, from 80 m to the top of the section, the percentage of smectite layers in IS R0 seems to increase again up to ~70% (Supplementary Data A).

4.1.4. El Kef – El Djebil section

In the sediments from El Kef – El Djebil section, the evolution of the clay fraction, again dominated by smectitic minerals, is divided into several mineralogical zones (Fig. 3; Supplementary Data F). Traces of illite are recorded in most samples. By contrast, kaolinite and chlorite are more abundant in 3 intervals. In the first interval, from 0–60 m, the percentages of kaolinite and chlorite diminish and these minerals disappear upward. In the second interval, from 80–330 m, the proportion of kaolinite increases to a maximum of 10% around 180 m, and then decreases progressively to 330 m. Chlorite shows a similar trend, with maximum values of around 5% at 180 m. Interestingly, the highest percentages of chlorite and kaolinite occur at the transition between the lower white chalks and the bioturbated marls. In the third interval, from 410–430 m, the proportion of kaolinite again rises up to 10%, along with traces of chlorite, and then falls from 430–465 m. However, the values in the third interval must be interpreted with caution, because of the high proportion of Si which distorts the peak area on the diffractogram required for percentage calculation (Si/Al ratio determined by an ICP-AES by Mabrouk El Asmi, 2014; Fig. 3).

4.2. Isotope analyses

4.2.1. Gubbio – la Bottaccione section

Bulk-rock $\delta^{13}C$ values range from about 2.1 to 2.7‰ through the Gubbio – la Bottaccione section (Fig. 4; Supplementary Data B). Three moderate isotopic excursions may be identified. From 1.2–9.5 m, a 0.3‰ positive shift is observed at the Santonian–Campanian transition and the C34/C33r chron boundary. A second positive shift of 0.4‰ starts at 23.8 m and ends at 40.3 m, before the first exposure gap, at the base of the *Contusotruncana*

446 *plummerae* zone. After increasing from 2.3 to 2.6‰ up to 61 m, $\delta^{13}C$ values decrease down to
447 about 2.4‰ up to 83 m. This decrease mostly occurs in the *Radotruncana calcarata* zone and
448 the upper part of chron C33n. From 95.8 m to the top of the section, the bulk-rock $\delta^{13}C$ values
449 display a decreasing trend of 0.2‰, which coincides with the Campanian–Maastrichtian
450 transition, within the *Gansserina gansseri* zone.
451 Bulk-rock $\delta^{18}O$ values display an increasing trend from values of about -3.0‰ at the base
452 of the Gubbio – la Bottaccione section, to values of about -2.2‰ around 40 m, and do not
453 show any further trend for the remaining of the section (Fig. 4; Supplementary Data B).
454
455 4.2.2. Furlo – Upper Road section
456
457 Bulk-rock $\delta^{13}C$ values range from about 2.0 to 2.9‰ in the Furlo – Upper Road section
458 (Fig. 4; Supplementary Data A). Between 1.3 and 5.9 m, a first two-step positive excursion of
459 0.4‰ coincides with the C34/C33r chron boundary and the Santonian–Campanian transition.
460 This excursion is followed by a negative excursion of about 0.4‰ with $\delta^{13}C$ values reaching
461 2.2‰ at 17 m. An increase in $\delta^{13}C$ values is then recorded, with maximum values of about
462 2.9‰ at about 30 m. From about 30 m to 44 m, the data show an overall decreasing trend
463 from values of about 2.9‰ to values of about 2.6‰, with one sample at the top of the interval
464 displaying a value of 2.4‰. It can be noted that this interval coincides with the first
465 occurrence of turbidites.
466 Above the 12 m-thick slump in the middle part of the studied section, bulk-rock $\delta^{13}C$ data
467 decrease from values of 2.6‰ at 56.7 m to values on average 2.3‰ at 92 m. This trend is
468 interrupted by a two-step negative excursion of 0.5‰, from 57.7 to 65.5 m, and from 65.5 to
469 72.5 m, occurring in the middle of chron C33n. Above 92 m, following a small positive
470 excursion of about 0.2‰, $\delta^{13}C$ values decrease again upwards, from $\delta^{13}C$ values of 2.5‰ at

93 m, and down to minimum values of 2‰ at the top of the section. The onset of this decrease coincides with the C33n1r/C32n2n chron boundary.

The $\delta^{18}O$ values remain quite stable in the lower part of the section, from the base to 44 m, with values around -2‰ on average (Fig. 4; Supplementary Data A). In the upper part of the section, they display a slight increase, from values of about -2‰ to values of about -1.5‰ around 80 m, before decreasing again to about -2‰ at the top of the section.

4.3. Nannofossils bioevents and biozonation of El Kef

A total of 17 samples of the El Kef section were studied here. Sample 81 (98.55 m) was barren, but the remainder of the samples yielded numerous late Cretaceous specimens. In total 61 individual calcareous nannofossil species were recognized in this study, a number which is rather low for the Campanian as this stage is characterised by the highest species richness of the whole Mesozoic (Bown, 2004). The low diversity recorded in El Kef section is likely the result of the preservation of the assemblage that is at best moderate. *Watznaueria barnesiae*, *Cribrosphaerella ehrenbergii*, *Prediscosphaera cretacea* and *Zeugrhabdotus bicrescenticus* are common.

The studied samples belong to the interval from zone CC18-CC19 to CC24 of Sissingh (1977) and $UC14a^{TP}$-$UC15b^{TP}$ to UC18 of Burnett (1998) due to the presence of *Broinsonia parca constricta* in the first sample (K1, 2.2 m) and the HO of *Tranolithus orionatus* in sample K447 (474.6 m). According to this applied biozonation, the age of the studied interval should range from the late early Campanian to early Maastrichtian. However, the inconsistency in the order of last occurrences recorded in the upper part of the section with respect to global schemes as well as with respect to other stratigraphic considerations, suggests that the zonations are hardly applicable to the section and that the whole studied

succession remains restricted to the Campanian only (see Discussion). A summary of the main results is provided in Fig. 5 (range chart with zonation and bioevents).

5. Discussion

5.1. Influence of diagenesis

A prerequisite for the use of clay minerals for palaeoenvironmental reconstructions is that they should mainly have a detrital origin. Smectitic minerals, which are the background of clay sedimentation in most latest Cretaceous open marine environments, are very sensitive to burial diagenesis. Illitization processes start when the temperature reaches about 60°C, (Kübler and Jaboyedoff, 2000; Kübler and Goy-Eggenberger, 2001) and IS R0 are progressively transformed into I/S R1, then R3, and finally into illite (Środoń, 2009). In each studied section, the illitization process is considered as subsidiary because of the high abundance of IS R0 throughout the successions (Supplementary Data A, B, C, D, E, F; Delissanti et al., 2010). In addition, low T_{max} values, comprised between 402° and 433°C, have been determined in previous studies for the "Bonarelli level" (OAE 2) of the Furlo section (Scaglia Rossa Formation), that corresponds to the immature zone of the organic matter, thereby suggesting negligible burial diagenesis consistent with persistence of IS R0 (Mort et al., 2007; Delissanti et al., 2010).

The $\delta^{13}C$ values of sediments from the Gubbio – la Bottaccione and Furlo – Upper Road sections comprised between 2.0 and 3.0‰, match $\delta^{13}C$ values typically observed in latest Cretaceous marine sediments of the Boreal and Tethyan realms (Jenkyns et al., 1994; Jarvis et al., 2002; Voigt et al., 2012; Figs. 6, 7). A cross-plot between $\delta^{13}C$ and $\delta^{18}O$ values shows close agreement for carbon between Furlo and Gubbio but a difference in oxygen, with

samples from Gubbio presenting lower values. A Spearman's coefficient was computed for each dataset to test the existence of a correlation within the data of each section. This method was chosen because of the non-linear nature of the relationship between the two variables, $\delta^{13}C$ and $\delta^{18}O$ (Chenot et al., 2016). A value of 1 indicates a perfect correlation, a value of -1 a perfect anti-correlation, while 0 indicates an absence of correlation. The two datasets generate Spearman's coefficients of r_s = -0.66 for Furlo and r_s = +0.11 for Gubbio (Fig. 6), pointing to an absence of a significant correlation between $\delta^{13}C$ and $\delta^{18}O$ values within each dataset.

The isotope data do not exhibit any inverted J curve in $\delta^{13}C$–$\delta^{18}O$ space that could reflect diagenesis involving fluid-rock interactions in addition to physical mixture of different diagenetic mineral phases (e. g. Bishop et al., 2014). This supports an absence of extensive diagenesis affecting both isotopic systems, and argues in favour of a preservation of $\delta^{13}C$ values. By contrast, the markedly lower $\delta^{18}O$ values recorded at Gubbio, which presents a deeper depositional environment compared to Furlo, likely indicate an impact of diagenesis on oxygen isotopes, although probably limited considering that the values fall within the range of shallow buried pelagic carbonate successions of comparable age elsewhere (e.g. Voigt et al., 2010; Fig. 7).

5.2. Identification and redefinition of carbon-isotopic events

In order to correlate the studied sections and boreholes, we used seven carbon-isotopic events, namely the: (1) Santonian–Campanian Boundary Event; (2) *papillosa* Zone Event; (3) Mid-Campanian Event; (4) Conica Event; (5) Late Campanian Event; (6) Epsilon Event and (7) Campanian–Maastrichtian Boundary Event, described in Section 3.3 (Fig. 8; Table 2).

545 5.2.1. Identifications of carbon-isotopic events in the Gubbio – la Bottaccione and Furlo –
546 Upper Road sections
547
548 A 0.4‰ positive shift in the basal Gubbio – la Bottaccione section (between 1.2 and 9.5 m)
549 and a two-step positive carbon-isotopic excursion of 0.4‰, recorded on the Furlo – Upper
550 Road section (between 1.3 and 5.9 m), coincide with the Santonian–Campanian transition and
551 the C34/C33r chron boundary respectively and are therefore attributed to the SCBE (Figs. 4;
552 8).
553 A sharp increase of 0.4‰ in the $\delta^{13}C$ curve identified within the mid-Lower Campanian in
554 the Gubbio – la Bottaccione section, starting at the base of the chron C33n and ending at the
555 base of the *Contusotruncana plummerae* zone, is assigned to the *papillosa* Zone Event (cf.
556 Thibault et al., 2016b; Sabatino et al., 2018). This excursion is not visible in the Furlo –
557 Upper Road section profile where it may be obscured or missing due to the slump interval
558 (Figs. 4, 8).
559 The MCE has been previously well-defined on the Bottaccione section, occurring above
560 the LOs of *Rucinolithus magnus* and *Uniplanarius gothicus*, but is not recorded on the
561 isotopic curve of this study, maybe because of the low amplitude of this isotopic event,
562 around 0.2‰ (Thibault et al., 2016b; Sabatino et al., 2018).
563 The LCE is well defined in the Gubbio – la Contessa section (Voigt et al., 2012) and in the
564 Gubbio – la Bottaccione section (Sabatino et al., 2018; Figs. 4, 8) with an amplitude of around
565 0.4‰. However, in this study, the LCE seems to be poorly expressed on our Gubbio – la
566 Bottacione profile, likely because of the occurrence of several gaps in the sedimentary record
567 of this section. However, the decreasing trend of 0.25‰ from 61 to 83 m identified in the la
568 Bottaccione section in the upper part of the chron C33n, including the *Radotruncana*
569 *calcarata* zone (Figs. 4, 8), is tentatively associated to the target horizon where the LCE could

570 be expected. In the Furlo – Upper Road section, the two-step negative excursion of 0.5‰,
571 above the 12 m-thick slump and occurring in chron C33n may be ascribed to the pre-LCE and
572 main-LCE (Figs. 4, 8).
573 The onset of the CMBE is well represented in both the Gubbio – la Bottaccione (starting at
574 98.5 m) and Furlo – Upper Road (starting at 94.1 m) sections (Figs. 4, 8).
575
576 5.2.2. Identification and attribution of carbon-isotope events from other sections
577
578 5.2.2.1. El Kef – El Djebil section
579
580 The calcareous nannofossil record of the upper part of the El Kef section (335 to 496
581 m) is difficult to interpret. Voigt et al. (2012, Fig. 6) documented a consistent succession of
582 closely spaced nannofossil HOs that occur in the Lower Maastrichtian at Gubbio and
583 Lägerdorf-Kronsmoor-Hemmoor, all within the upper part (their intervals 3 – 5) of the
584 CMBE: *U. trifidus*, *B. parca constricta*, *T. orionatus*. The consecutive datum levels lie on a
585 marked falling trend in the $\delta^{13}C$ curve, which precedes a sharp rise in values towards the Mid-
586 Maastrichtian Event (MME), above. The same succession of nannofossil disappearances at El
587 Kef are spread through >100 m of the Ncham Chalk, largely within an interval of relatively
588 high $\delta^{13}C$ values (Figs. 3, 8) above the negative excursion defining the LCE.
589 The HO of *U. trifidus* has been recently considered as the best nannofossil marker for
590 the Campanian/Maastrichtian boundary and was used to subdivide UC zone 16 into subzones
591 $UC16a^{TP}$ and $UC16b^{TP}$ (Thibault, 2016). The HO of *U. trifidus* at 403 m would thus suggest
592 that this boundary lies close to that stratigraphic height, and that the negative excursion
593 recorded between 339 and 390 m corresponds to the CMBE, not the LCE. However, the HO
594 of *B. parca constricta*, which marks the top of UC18 and should thus be recorded higher up at

El Kef was found here below the HO of *U. trifidus*. Moreover, a narrow range of the curved spine nannolith at El Kef, straddling the negative excursion, contradicts other nannofossil results and the identification of this excursion as the CMBE. Indeed, the HO of the curved spine is generally restricted to the late Campanian, and correlates to the top of the LCE (Thibault et al., 2012a; Thibault, 2016; M.R. Razmjooei and N. Thibault, pers. comm., unpublished results from Iran). It is therefore possible that the HOs of *B. parca constricta* and *U. trifidus*, which are nearly identical between El Kef (this study) and Kalaat Senan (Robaszynski et al., 2000) are recorded in the region of the Kasserine Island much earlier than in the rest of the Tethys due to local environmental conditions.

The negative $\delta^{13}C$ excursion between 339 and 390 m at El Kef lies in the upper part of the Akhdar Marl Member *sensu* Jarvis et al. (2002). Robasyzynski et al. (2000) recorded the Upper Campanian ammonite *Nostoceras (Nostoceras) hyatti* above this in the lowest part of the overlying Ncham Chalk Member. The index ammonite taxon *Nostoceras (Bostrychoceras) polyplocum* ranges through the lower part of the Akhdar Marl, overlapping with the base of the *G. calcarata* foraminifera Zone, above. The negative $\delta^{13}C$ excursion occurs above the top of the *G. calcarata* Zone and below the base *N. hyatti*. This stratigraphic relationship between the excursion and the macrofossil datum levels is essentially identical to that recorded for the Late Campanian Event (LCE) in the Tercis-les-Bains GSSP by Voigt et al. (2012), and is well below the base of the CMBE. These data support the original interpretation of Jarvis et al. (2002) that the negative $\delta^{13}C$ excursion at El Kef is the LCE not the CMBE.

The planktonic foraminifera biostratigraphy is not definitive: *G. gansseri* occurs very infrequently at its lowest occurrence at Kalaat Senan (Robaszynski et al. 2000, Figs. 3, 8), and is only recorded consistently in the boundary interval between the Akhdar and Ncham Members ('Gorbeuj Member' of Robaszynski et al. 2000). The first consistent occurrence

correlates to above the negative excursion at El Kef (Jarvis et al. 2002, Fig. 2). Unfortunately, *G. gansseri* was not identified in the low-resolution foraminifera study of El Kef (El Djebil) by De Cabrera (in Jarvis et al. 2002).

Finally, attributing the main negative excursion at El Kef to the CMBE rather than the LCE would necessitate major changes in sedimentation rate within the section that are not supported by coincident lithological variation, and/or challenges the stratigraphic completeness of the logged succession. In conclusion, we retain here the original carbon isotope event assignments of Jarvis et al. (2002), while acknowledging the challenges of the stratigraphy that warrant further study.

5.2.2.2. Cbr-7 borehole

The short 1‰ negative excursion of $\delta^{13}C$ measured by Richard et al. (2005) in the Cbr-7 borehole (Figs. 3, 8) was not ascribed to any recognized isotopic event. The Mn peak observed in this borehole corresponds to a glauconite-bearing hardground, which points to the existence of a condensed interval and/or hiatus, consistent with Mn accumulation. In this case, the 1‰ excursion recorded in $\delta^{13}C$ values may correspond to the LCE, according to its occurrence within the lower part of the upper Campanian.

However, the hardground at the summit of the Trivières Chalk occurs in the basal *Belemnitella mucronata* zone (Robaszynski et al., 2001; Richard et al., 2005), i.e. very close to the base of the Upper Campanian as calibrated in NW Europe. Interestingly, a succession of hardgrounds occurs at a very similar stratigraphic level in the Trunch borehole of Eastern England, called the Trunch Hardgrounds by Jarvis et al. (2002). The MCE is placed immediately above this condensed interval in the Trunch borehole. If these hardgrounds are equivalent to the Trivières hardground, then the negative $\delta^{13}C$ excursion in the Cbr-7 borehole

correlates to the negative excursion immediately below the Trunch Hardgrounds, and the small peak above the negative excursion in Cbr-7 would be the MCE. Decreasing-upward values at the top of Cbr-7 in the Nouvelles Chalk can then be interpreted to represent the lower part of the LCE, which we used in this study for the stratigraphic correlation (Figs. 3, 8).

5.3. Clay minerals origin in the Tethyan realm

The origin of smectitic minerals in oceanic sediments is controversial and has been debated by Chamley (1989) and Thiry (2000). The abundance of these minerals in Cretaceous sediments, especially from cores drilled in the Atlantic Ocean, is interpreted differently by the authors. Smectitic minerals are considered to be detrital in some studies, based on their chemical composition (Al-Fe beidellite), which is similar to smectitic minerals formed in soils, on their REE element profiles, and on their strontium isotope composition (see Chamley, 1989; Chamley et al., 1990). Alternatively, a volcanogenic or early diagenetic origin of smectitic minerals has been proposed based on the common occurrence of the paragenesis smectite opal-CT-clinoptilolite (Pomerol and Aubry, 1977; Christidis, 1995; Madsen and Stemmerik, 2010). The controversy also arises from the coeval occurrence of smectite-poor continental successions and smectite-rich marine sediments. This paradox has been tentatively explained by the massive neoformation of smectitic minerals in oceanic basins or by the transformation of detrital clay particles into smectitic minerals (Thiry and Jacquin, 1993). Other authors have suggested that differential settling processes are responsible for the smectitic minerals enrichment in (hemi-) pelagic environments (Chamley, 1989).

669 In the clay fraction of the Upper Cretaceous Chalk, it is now clear that the smectitic
670 minerals correspond to a mixture of detrital I/S, authigenic lathed smectitic minerals
671 preferentially formed in slowly deposited sediments, and smectitic minerals deriving from the
672 submarine weathering of volcanic glass shards (Deconinck and Chamley, 1995; Jeans, 2006).
673 Environmental conditions during the Late Cretaceous favoured dominantly smectitic
674 sedimentation: high sea level; low topographic relief on continental areas; relatively
675 seasonally contrasted humid climate; low sedimentation rates; and recurrent volcanism
676 expressed by the common occurrence of bentonite layers (Chamley et al., 1990; Deconinck
677 and Chamley, 1995).

678 Chlorite and illite are generally directly reworked from igneous or metamorphic
679 continental basement rocks and are therefore commonly considered to be primary minerals
680 (Chamley, 1989; Weaver, 1989; Ruffell et al., 2002). Consequently, their proportions increase
681 either during tectonic rejuvenation, sea-level fall, or under dry climate when chemical
682 weathering is reduced. By contrast, the pedogenic formation of kaolinite occurs under warm
683 and humid conditions suitable for high rates of chemical weathering (Ruffell et al., 2002).
684 However, this mineral may be also reworked together with primary minerals (e.g. illite,
685 chlorite) from ancient kaolinite-bearing sedimentary rocks (Deconinck and Vanderaveroet,
686 1995). In that case, kaolinite cannot be used as evidence for the existence of humid climate.
687 Coupling or decoupling in the variation of primary minerals and of kaolinite, however, may
688 help differentiate between pedogenic vs. reworked origins, thereby indicating the reliability of
689 kaolinite as a palaeoclimate indicator.

690 An important feature that is highlighted by clay mineral assemblages of the studied
691 sections is the absence of significant amounts of kaolinite in the northernmost sections located
692 in the Danish basin and the North Sea (Fig. 9). By contrast, kaolinite occurs in the three
693 sections located south of 30°N (El Kef – El Djebil and Umbria-Marche localities). The two

694 sections located latitudinally in-between, in the Paris and Mons basins, present intermediate
695 characteristics with kaolinite present in the Cbr-7 borehole, but absent in the Poigny borehole.
696 This broad latitudinal zonation may result from a climatic control, as humid/arid conditions
697 are known to impact clay mineral assemblages (Ruffell et al., 2002; Dera et al., 2009). The
698 common occurrence of bauxite reported in the general area of Gubbio, Furlo, and Tercis-les-
699 Bains (Bárdossy and Dercourt, 1990), supports at least a partial pedogenic origin of kaolinite
700 observed in these sections (Fig. 10).

701 Based on the distribution of kaolinite and bauxite along the palaeolatitudinal transect,
702 climatic zones are proposed in the Tethyan/Boreal realms during the Campanian (Figs, 10,
703 11). Between 20° and 35°N, the clay fractions are characterised by the occurrence of kaolinite
704 and iron (oxyhydro)oxides (e.g. hematite in the Scaglia-Rossa Formation; Channell et al.,
705 1982), corresponding to intense weathering under warm and humid climate conditions. These
706 climatic conditions are also highlighted by the distribution of Late Cretaceous bauxites which
707 are abundant in southern France and in the Dinarides at palaeolatitudes below 35°N (Charvet,
708 1978; Bárdossy and Dercourt, 1990; D'Argenio and Midszenty, 1995; Fig. 10). North of
709 35°N, clay assemblages are mainly dominated by smectitic minerals and illite (with traces of
710 chlorite and kaolinite), and the absence of bauxite indicates limited chemical weathering,
711 consistent with seasonally contrasted climate.

712 However, variations in primary mineral proportions (chlorite and illite) mirror those of
713 kaolinite, pointing to the additional presence of reworked kaolinite. A similar co-variation of
714 primary minerals and kaolinite is identified at El Kef, again suggesting the predominance of
715 kaolinite reworked from old rocks that cropped out on nearby emergent landmasses. To our
716 knowledge, no major bauxite deposits are reported for the Upper Cretaceous in that area
717 (Tardy et al., 1991; Monsels, 2016), which was located in an arid zone according to the
718 distribution of vegetation (Otto-Bliesner and Upchurch, 1997; Chumakov, 2004). These

observations suggest that kaolinite is dominantly reworked together with primary minerals in all sections south of 30°N. Consequently, clay sedimentation was not solely controlled by climate but involved an additional factor, which could be linked to the tectonic instability of the southern margin of the Tethys, or to the long-term trend of sea-level fall that characterises the Late Cretaceous.

5.4. Diachronous fluctuations of detrital clay minerals with palaeolatitude

A striking feature arising from the overall clay mineralogical results of all studied sections is the earlier occurrence of kaolinite on southern Tethyan margin sites compared to the northern domain (Fig. 9). At El Kef, three intervals of increased detrital minerals (chlorite and kaolinite) are recorded: from the transition between the lower to middle Campanian (within CC19 and the lower part of CC20 nannofossil biozones); from the base of CC21 to the top of the *Radotruncana calcarata* foraminifera zone; and from the base to the top of CC23 (Fig. 3). In the Umbria-Marche basin, the onset of detrital input of clay minerals occurs in youngest sediments dated to the upper part of the middle Campanian (Fig. 4). At Tercis-les-Bains, illite and kaolinite contents increase at the base of the pre-LCE, while a coeval increase of illite is recorded in the Paris Basin (Poigny borehole; Chenot et al., 2016, Fig. 9). Consequently, the studied sections point to a general increase in detrital input during the Campanian that is diachronous, with an earlier onset in the southern sections (El Kef, Furlo, Gubbio) than those immediately to the north (Tercis-les-Bains, Poigny).

In the northernmost sections (Poigny, Adda-3 and Stevns-2), no clear trend is apparent in the abundance of detrital clay minerals, except for Cbr-7 (Fig. 9). At that site, an increase in detrital input is recorded by an increase in illite and talc proportions in the upper part of the borehole. This contrasts with the other sites where the increase in detrital inputs is marked by

744 increasing kaolinite proportions. This difference may result from a different climatic context
745 that is evidenced by the transition from kaolinite-bearing clay fraction at the base of the
746 borehole toward sediments containing palygorskite, suggesting an evolution from relatively
747 humid to more semi-arid conditions. It is however worth noting that a hardground separates
748 the two intervals in Cbr-7, pointing to the existence of a significant hiatus, the duration of
749 which cannot be evaluated because of the lack of biostratigraphic markers. The large
750 uncertainties on the stratigraphic framework preclude further temporal comparison of the
751 depicted increase in detrital inputs with that recorded at the other studied sites (Fig. 9).
752
753 5.5. A tectonic versus climatic control of clay sedimentation
754
755 Although the long-term sea-level fall recorded during the Late Cretaceous could have
756 contributed to the general increase in detrital inputs depicted here (Haq et al., 1988;
757 Hardenbold et al., 1998; Haq, 2014), their diachronism between sites strongly suggests the
758 existence of additional processes at play.
759 The Late Cretaceous was characterised by compressive events around the Tethys, linked
760 to the northward motion of Africa toward Eurasia (Kley and Voigt, 2008; Frizon de Lamotte
761 et al., 2011; Jolivet et al., 2016). During the Campanian – Maastrichtian interval, large areas
762 of emerged land and newly created relief in central Europe and in the western Tethyan realm
763 (e.g. southern Carpathians, east-Pyreneans, inverted Mid-Polish Anticline, High-Karst)
764 delivered detrital material to the adjacent sedimentary basins (Charvet, 1978; Willingshofer et
765 al., 2001; Kley and Voigt, 2008; Voigt et al., 2008; Melinte-Dobrinescu and Bojar, 2010;
766 Oms et al., 2016; Figs. 1, 10, 12).
767 On the southern Tethyan margin, evidence of tectonic instability as early as the earliest
768 Campanian, is suggested by the occurrence of synsedimentary faults, slumps and slope

769 instability features in sedimentary successions from northeastern Tunisia (Boutib et al., 2000;
770 Bey et al., 2012). This tectonically driven sedimentation persisted throughout the Campanian
771 and possibly into the Maastrichtian, as illustrated by syndepositional faulting and gravity flow
772 deposits in the Abiod Chalk (Bouaziz et al., 2002; Dlala 2002; Negra, 2016). In the
773 southernmost section of El Kef, the detrital influence occurring in the middle Campanian
774 might be linked to a tectonic rejuvenation of nearby continental areas (e.g. Kasserine Island,
775 Kadri et al., 2015; Figs. 1, 10, 12).

776 At El Kef, several kaolinite- and chlorite-enriched detrital intervals are recognised,
777 separated by intervals devoid of typical detrital minerals. This may reflect distinct tectonic
778 pulses affecting this segment of the southern margin (Figs. 3, 12). The kaolinite-rich interval
779 within the *G. ventricosa* zone at El Kef is coeval with the occurrence of rudist-bearing
780 olistolith beds on the NE margin of Kasserine Island (Negra et al., 2016), further highlighting
781 a phase of platform destabilisation.

782 In central Italy (Umbria-Marche basin), detrital input of kaolinite and chlorite started
783 later, in the earliest part of chron C33n (Figs. 4, 12). Volcanic activity in the area is
784 highlighted by the preservation of a bentonite layer in the *G. elevata* zone (more precisely in
785 the lower Campanian CC18 nannofossil biozone; Mattias et al., 1988; Fig. 4). The ashfall
786 originated from an active volcanic centre related to a subduction zone located to the east of
787 the Umbria-Marche basin, in the Dinarides (Charvet, 1978), and points to active tectonism in
788 this region (Bernoulli et al., 2004; Schmid et al., 2008). In the Furlo – Upper Road section, the
789 occurrence of the bentonite layer is followed by slope destabilisation features including
790 decimetric turbidite beds and a 12 m-thick slump, suggesting long-lasting tectonic instability
791 (Fig. 4).

792 Within the same tectonic and climatic context, additional differences in clay mineralogy
793 between geographically close sections are evidenced in the Umbria-Marche basin. Indeed, a

794 comparison between the Gubbio – la Bottaccione and Furlo – Upper Road sections shows that
795 kaolinite is more abundant at Furlo, which was located on a slope at shallower depth than
796 Gubbio (Fig. 4). This difference is emphasised by the occurrence of numerous slope deposits
797 including slumps and turbidites at Furlo, while basinal deposits characterised the Gubbio
798 section. This clay mineral distribution is attributed to differential settling of kaolinite which
799 likely originated from the east, possibly from the High Karst (Gibbs, 1977; Charvet, 1978;
800 Figs. 1, 12).

801 A local tectonic influence coinciding with the LCE is also recorded in the Tercis-les-
802 Bains section where chlorite, illite and kaolinite increase (Figs. 9–12). This detrital event is
803 likely due to a tectonic pulse linked to the Pyrenean compressional phase between Iberia and
804 southern Europe (Laurent et al., 2001; Vergés et al., 2002; Oms et al., 2016). A coeval event
805 characterised by increasing proportions of illite is recorded in the Paris Basin (Poigny
806 borehole, Deconinck et al., 2005; Figs. 9–12), potentially related to a compressive event
807 (Mortimore and Pomerol, 1997). Slump deposits recorded in the Anglo-Paris Basin in the
808 middle Campanian (Gale et al., 2015) could also relate to local tectonic instability.

809 By contrast, in the northern part of the studied transect, there are no clear detrital events
810 similar to those recorded in the southern sections, despite the presence of active tectonism in
811 this region affected by inversions at the time (Kley and Voigt, 2008; Voigt et al., 2008),
812 probably because this area was too far away from emerged areas (Figs. 9–12). Thus, the
813 climatic control on clay sedimentation is more clearly expressed at these sites. In the Mons
814 basin, during the late Campanian, the progressive decreasing proportion of kaolinite was
815 followed by the occurrence of palygorskite, which reflects the establishment of increasingly
816 semi-arid climatic conditions (Figs. 3, 9–12). However, traces of talc present in the late
817 Campanian could be related either to a change of detrital sources or to the generation of newly
818 exposed areas by the extensive coeval tectonism recorded in the basin (Vandycke and

819 Bergerat, 1989), which is consistent with the coevally increase of illite in this basin. In the
820 Danish North Sea, similar semi-arid to semi-humid climatic conditions are consistent with the
821 abundance of IS R0, which constitutes the entire clay fraction of uppermost Campanian
822 sediments (Figs. 2, 9–12).
823
824 5.6. Carbon cycle and continental weathering
825
826 Carbon cycle changes and continental weathering had been tentatively linked through
827 the observed correspondence between the carbon isotope excursion defining the LCE and
828 enhanced terrigenous inputs, identified by a coeval increase in kaolinite, chlorite and illite
829 proportions at Tercis-les-Bains and Poigny (Chenot et al., 2016). The new results presented
830 here, which include data from sections located over a wider range of palaeolatitude, show that
831 this relationship does not hold. Indeed, the diachronous nature of detrital supplies evidenced
832 here, interpreted as reflecting the northward progression of tectonic deformation, results in a
833 decoupling between the carbon-isotope excursions and the evolving clay minerals
834 assemblages.
835 However, our new clay mineralogical data highlight enhanced continental weathering
836 throughout the whole Campanian stage, with a diachronous onset from the south to the north
837 (Figs. 10, 12). As silicate weathering is known to promote atmospheric CO_2 drawdown
838 (Berner, 1990, 2004; Berner and Kothavala, 2001), our new data hint to a potentially major
839 role of incipient orogenic processes on Late Cretaceous long-term cooling. The data compiled
840 by Royer et al. (2012) and Franks et al. (2015) highlight lower pCO_2 levels in the Campanian
841 and Maastrichtian than during the Albian to Turonian interval, but the temporal resolution is
842 not sufficient to discuss correlations between pCO_2 fluctuations, tectonic phases and the
843 evolution of clay minerals assemblages depicted in our study. Decreasing atmospheric CO_2

844 levels during the Late Cretaceous have been repeatedly associated to reduced outgassing CO_2
845 flux from mid-ocean ridge volcanism and arc magmatism (Berner et al., 1983; Jones et al.,
846 1994; Godderis and François, 1995; Berner, 2004; McKenzie et al., 2016). Without excluding
847 the role of reduced CO_2 volcanic outgassing, our new results highlight an additional important
848 mechanism that may have contributed to the Late Cretaceous cooling. Although initiation of
849 the Tethyan closure began during the mid-Cretaceous, the Santonian–Campanian is marked
850 by a change of direction and faster motion of African toward Eurasia (Bosworth et al., 1999;
851 Guiraud and Bosworth, 1999; Frizon de Lamotte et al., 2011; Jolivet et al., 2016). The
852 Campanian is also characterised by an acceleration of the long-term climatic cooling recorded
853 during the Late Cretaceous (Cramer et al., 2009; Friedrich et al., 2012; Linnert et al., 2014),
854 which coincides with enhanced detrital inputs depicted by clay minerals in our study. This
855 temporal coincidence between an acceleration of cooling, tectonic pulses, and clay detrital
856 input evolution further argues for a significant impact on climate of plate tectonics linked to
857 Africa-Eurasia convergence. Although the importance of this process remains to be tested
858 quantitatively using geochemical models, our work opens new perspectives on the
859 understanding of the Late Cretaceous climate cooling.
860
861 ## 6. Conclusion
862
863 New results on clay minerals assemblages of Campanian sediments from six sections
864 and boreholes ranging from the southern Tethyan margin to the Boreal realm, provide the first
865 insights on the evolution of continental weathering at the Tethyan scale during a long
866 underexplored time interval (11 Myr).
867 We propose a climatic zonation in the west Tethyan to Boreal realms during the late
868 Campanian: (1) a semi-humid climate belt north of 35°N, based on the sporadic occurrence of

kaolinite, the occurrence of palygorskite and the high percentage of smectitic minerals; (2) a warm and humid climate belt, based on the occurrence of kaolinite and bauxite between 35°–20°N; and maybe (3) a semi-arid zone south of 20°N, adjacent to the Saharan platform, based on the abundance of smectitic minerals, with kaolinite interpreted here as being reworked from the basement.

Superimposed on this latitudinal climate distribution, we have identified detrital events in several basins. These events resulted from weathering of emerged continental areas, that we relate to the main tectonic active zones, and more specifically to the large subduction zone of the central Tethyan realm between African and Eurasian plate (Umbria-Marche basin, Furlo and Gubbio sections), the extensional basins in southern Tethys (Saharan platform margin, El Kef section), and the collision between the Iberian and the Eurasian plates (Aquitaine basin, Tercis-les-Bains section). These tectonic instabilities, associated with a warm and humid climate, likely led to enhanced chemical weathering of the newly created continental relief.

The northward migration of an enhanced detrital flux evidenced by our new records, linked to the progression of compressional deformation, reflects the closure of the Tethys due to the northward motion of Africa. As chemical weathering of silicate induces CO_2 consumption, we suggest that Late Cretaceous cooling was partly linked to enhance continental weathering.

7. Acknowledgments

This work was supported by the ANR Anox Sea and the Institut Universitaire de France (IUF). We are also grateful to Francis Robaszynski for the help with Cbr-7 borehole calibration, and Anne-Charlotte Guillet for her contribution in the lab.

FIGURES

Figure 1: Palaeogeography of the Campanian–Maastrichtian of the west Tethyan and south Boreal realms (modified from Philip and Floquet, 2000). Location of the sites studied: [A] Adda-3 borehole; [C] Cbr-7 borehole; [F] Furlo – Upper Road section; [G] Gubbio – la Bottacione section; [K] El Kef – El Djebil section; [P] Poigny borehole; [S] Stevns-2 borehole; [T] Tercis-les-Bains section. The green squares represent previously published data (Deconinck et al., 2005; Chenot et al., 2016) used in this study.

Figure 2: Stratigraphy and clay mineralogy of the Campanian–Maastrichtian in northern boreholes. (A) Clay mineralogical data (this study) of the Adda-3 borehole compared to the gamma-ray and carbon- and oxygen-isotopic data (Perdiou et al., 2016). (B) Clay mineralogical data (this study) from Stevns-2 borehole compared to gamma-ray and carbon- and oxygen- isotopic data (Boussaha et al., 2016).

Figure 3: Stratigraphy and clay mineralogy of the Campanian in the Mons basin, Belgium and Campanian–Maastrichtian at El Kef, Tunisia. (A) Clay mineralogical data from the Cbr-7 borehole and carbonate content (this study) compared to carbon- and oxygen-isotope data and manganese contents (ppm) (Richard et al., 2005). (B) Clay mineralogical data from the El Kef – El Djebil section (this study), compared to carbon- and oxygen- isotopic data (Jarvis et al., 2002), carbonate content and Si/Al ratio (Mabrouk El Asmi, 2014). The foraminiferal biostratigraphic data of El Kef – El Djebil section are established from the lithostratigraphic comparison with Kalaat Senan section (see Jarvis et al., 2002), while the calcareous nannofossil biostratigraphic data have been performed on the El Kef – El Djebil samples.

G. aegyptica = *Globotruncana aegyptica*; *G. elevata* = *Globotruncanita elevata*; *G. f.* = *Globotruncana falsostuarti*; *G. h.* = *Globotruncanella havanensis*; *G. g.* = *Gansserina gansseri*; *G. ventricosa* = *Globotruncana ventricosa*; *R. calcarata* = *Radotruncana calcarata*

A. c. var NT = Arkhangelskiella cymbiformis; A. c. var W = Arkhangelskiella cymbiformis var W; B. p. c. = Broinsonia parca constricta; C. spine = curved spine nannolith*; E. e. = Eiffellithus eximius; M. cf. M. p. = Micula cf M. premolisilva; R. a. = Reinhardites anthrophorus; T. o. = Tranolithus orionatus; U. g. = Uniplanarius gothicus; U. s. = Uniplanarius sissinghii; U. t. = Uniplanarius trifidius.*

Figure 4: Stratigraphy and clay mineralogy of the Campanian in the Umbria-Marche basin, Italy. Clay mineralogical data (this study) compared to carbon- and oxygen- data (this study) from (A) Gubbio – la Bottaccione and (B) Furlo – Upper Road sections. Magnetostratigraphy of Gubbio – la Bottaccione from Lowrie and Alvarez (1977); Furlo – Upper Road from Alvarez and Lowrie (1984). Gubbio biostratigraphic data from Coccioni and Premoli Silva (2015).

A. m. = Archaeglobigerina minimus; *D. a. = Dicarinella asymetrica*; *E. e. = Eiffellithus eximius*; *G. a. = Globotruncana aegyptica*; *G. e. = Globotruncanita elevata*; *G. h. = Globotruncanella havanensis*; *G. gansseri = Gansserina gansseri*; *G. st. = Globotruncanita stuarti*; *G. v. = Globotruncana ventricosa*; *R. l. = Reinhardites levis*; *R. m. = Rucinolithus magnus*; *U. g. = Uniplanarius gothicus*; *U. t. = Uniplanarius trifidus.*

Figure 5: Occurrence of selected calcareous nannofossils taxa in El Kef – El Djebil section.

Figure 6: Cross-plot of carbon- and oxygen-isotope bulk-rock data of the Gubbio – la Bottaccione and Furlo – Upper Road sections.

Figure 7: Cross-plot of carbon- and oxygen-isotope bulk-rock data of the Gubbio – la Bottaccione (▲) and Furlo – Upper Road (▲) sections compared with isotopic data from several sites in the Tethyan Realm (A) to the north of 35 °N and (B) to the south of 35 °N.

Figure 8: Correlation of the $\delta^{13}C$ profiles across the Campanian between Adda-3 (Perdiou et al., 2015), Stevns-2 (Boussaha et al., 2016), Cbr-7 (Richard et al., 2005), Poigny borehole (Chenot et al., 2016), Tercis-les-Bains section (Voigt et al., 2012), Gubbio – la Bottaccione

943 section (this study), Furlo – Upper Road section (this study) and El Kef – El Djebil section
944 (Jarvis et al., 2002).
945 **Figure 9:** Comparison of clay mineralogical assemblages of Campanian sediments of the sites
946 studied (smectitic minerals are not represented). Correlation based on carbon-isotope events,
947 along a palaeolatitudal transect from ~20°N to ~40°N. Adda-3 borehole, clay mineralogical
948 data (this study) compared to the carbon- isotopic data (Perdiou et al., 2016); Stevns-2
949 borehole, clay mineralogical data (this study) compared to carbon- isotopic data (Boussaha et
950 al., 2016); Cbr-7 borehole, clay mineralogical data (this study) compared to carbon- isotopic
951 data (Richard et al., 2005); Poigny borehole, clay mineralogical data compared to carbon-
952 isotopic data (Chenot et al., 2016); Tercis-les-Bains section, clay mineralogical data (Chenot
953 et al., 2016) compared to carbon–isotopic data (Voigt et al., 2012); Gubbio – la Bottaccione,
954 clay mineralogical data compared to carbon- isotopic data (this study); Furlo – upper Road
955 section, clay mineralogical data compared to carbon- isotopic data (this study); El Kef – El
956 Djebil section, clay mineralogical data (this study) compared to carbon – isotopic data (Jarvis
957 et al., 2002).
958 **Figure 10:** Geodynamic framework of Campanian Tethyan bauxites and the clay minerals of
959 the studied sections (modified from Bárdossy and Dercourt, 1990; Jolivet et al. 2016).
960 Location of the sites studied: [A] Adda-3 borehole; [C] Cbr-7 borehole; [F] Furlo – Upper
961 Road section; [G] Gubbio – la Bottaccione section; [K] El Kef – El Djebil section; [P] Poigny
962 borehole; [S] Stevns-2 borehole; [T] Tercis-les-Bains section.
963 Name of the Campanian bauxites localities: (1) Alpilles (France), (2) Haut-Var (France), (3)
964 Markusovce (Slovakia), (4) La Boissière (France), (5) Nurra (Sardinia), (6) Villeveyrac basin
965 (France), (7) Bédarieux (France), (8) Tyrol Brandenberg and Salzburg (Austria), (9)
966 Unterlaussa (Austria), (10) Sümeg (Hungary), (11) Halimba (Hungary), (12) Ihakut-
967 Németbanya (Hungary), (13) Grméc Hill (Bosnia Herzegovina), (14) Jajce (Bosnia

968 Herzegovina), (15) Grebnik (Kossovo), (16) Kücük Koras, Sebimlkoy (Turkey), (17) Payas,
969 Islaye (Turkey), (18) Sohodol, Cimpeni (Romania), (19) Euboea Island (Greece).
970 **Figure 11:** (A) Palaeolatitudinal topographic profile for the studied sites and their positions
971 relative to the main orogenic belt during the studied time interval (see also Fig. 10) compared
972 with (B) a reconstruction of the latitudinal climatic zonation with the locations of major
973 bauxites. These provide a potential source of hydrolytic minerals into the adjacent
974 sedimentary basin during the Santonian–Maastrichtian interval. (C) Palaeolatitudinal transect,
975 from the base of the Late Campanian Event to the top of the end of late Campanian, of the
976 mean clay minerals assemblages from sites studied in the Tethyan and Boreal realms.
977 Location of the sites studied: [A] Adda-3 borehole; [C] Cbr-7 borehole; [F] Furlo – Upper
978 Road section; [G] Gubbio – la Bottacione section; [K] El Kef – El Djebil section; [P] Poigny
979 borehole; [S] Stevns-2 borehole; [T] Tercis-les-Bains section. There is no direct
980 correspondence between A and B frames; the formation of bauxite and kaolinite occurred in
981 humid tropical conditions. The synthetic "orogenic belt" (defined in A) represents both the
982 Pyrenees and Alpine units that have their own geodynamic histories.
983 **Figure 12:** Scenario of the African block rotation modification, placed on a palaeogeographic
984 map of the west Tethyan – south Boreal realm, from the end of the Santonian to the late
985 Campanian. Histograms illustrate the proportion of clay mineral species (excluding the
986 smectitic minerals background sedimentation) at the sites studied, during the (A) end
987 Santonian, (B) early Campanian to early mid-Campanian, (C) later mid-Campanian, (D) Late
988 Campanian Event, and (E) late Campanian.
989

990 **TABLES**

991 **Table 1:** Peak positions used for the recognition of clay minerals (>2 μm) of the insoluble
992 residue.

993 **Table 2**: Synthesis of carbon-isotope events recognised in the Campanian.

994

SUPPLEMENTARY DATA

Supplementary Data A: Carbon and oxygen isotopes of the bulk rock, lithology and clay mineralogy of the Furlo – Upper Road section.

Supplementary Data B: Carbon and oxygen isotopes of the bulk rock, calcium carbonate content, lithology and clay mineralogy of the Gubbio – la Bottaccione.

Supplementary Data C: Carbon and oxygen isotopes of the bulk rock, calcium carbonate content, lithology and clay mineralogy of the Cbr-7 borehole.

Supplementary Data D: Carbon and oxygen isotopes of the bulk rock, lithology and clay mineralogy of the Stevns-2 borehole.

Supplementary Data E: Carbon and oxygen isotopes of the bulk rock, lithology and clay mineralogy of the Adda-3 borehole.

Supplementary Data F: Carbon and oxygen isotopes of the bulk rock, calcium carbonate content, lithology and clay mineralogy of the El Kef – El Djebil section.

REFERENCES

Açıkalın, S., Vellekoop, J., Ocakoğlu, F., Yılmaz, I.Ö., Smit, J., Altıner, S.Ö., Goderis, S., Vonhof, H., Speijer, R.P., Woelders, L., 2015. Geochemical and palaeontological characterization of a new K-Pg Boundary locality from the Northern branch of the Neo-Tethys: Mudurnu–Göynük Basin, NW Turkey. Cretaceous Research 52, 251–267.

Alvarez, W., Lowrie, W., 1984. Magnetic stratigraphy applied to synsedimentary slumps, turbidites, and basin analysis: the Scaglia limestone at Furlo (Italy). Geological Society of America Bulletin 95 (3), 324–336. doi:10.1130/0016-7606(1984)95<324:MSATSS>2.0.CO;2.

Aris, Y., Coiffait, P.E., Guiraud, M., 1998. Characterisation of Mesozoic–Cenozoic deformations and palaeostress fields in the Central Constantinois, northeast Algeria. Tectonophysics 290, 59–85.

Arthur, M.A., Fischer, A.G., 1977. Upper Cretaceous–Paleocene magnetic stratigraphy at Gubbio, Italy I. Lithostratigraphy and sedimentology. Geological Society of America Bulletin 88 (3), 367–371. doi:10.1130/0016-7606(1977)88<367:UCMSAG>2.0.CO;2.

Bárdossy, G., Dercourt, J., 1990. Les gisements de bauxites téthysiens (Méditerranée, Proche et Moyen Orient); cadre paléogéographique et contrôles génétiques. Bulletin de la Société Géologique de France 6 (6), 869–888.

Berner, R.A., 1990. Atmospheric carbon dioxide levels over Phanerozoic time. Science 249, 1382–1386.

Berner, R.A., 2004. The Phanerozoic Carbon Cycle: CO_2 and O_2. Oxford University Press, Oxford, 158 pp.

Berner, R.A., Lasaga, M., Garrels, R.M., 1983. The carbonate-silicate geochemical cycle and its effect on atmospheric CO_2. American Journal of Science 283, 641–683.

1033 Bernoulli, D., Schaltegger, U., Stern, W.B., Frey, M., Caron, M. Monechi, S., 2004. Volcanic
1034 ash layers in the Upper Cretaceous of the Central Apennines and a numerical age for the
1035 early Campanian. International Journal of Earth Sciences 93 (3), 384–399.
1036 Bey, S., Kuss, J., Premoli Silva, I., Negra, H., Gardin, S., 2012. Fault-controlled stratigraphy of
1037 the Late Cretaceous Abiod Formation at Ain Medheker (northeast Tunisia). Cretaceous
1038 Research 34, 10–25. doi:10.1016/j.cretres.2011.09.008.
1039 Bishop, J.W., Osleger, D.A., Montañez, I.P., Sumner, D.Y., 2014. Meteoric diagenesis and
1040 fluid-rock interaction in the Middle Permian Capitan backreef: Yates Formation, Slaughter
1041 Canyon, New Mexico. AAPG Bulletin 98, 1495–1519.
1042 Blakey, R.C., 2008. Gondwana paleogeography from assembly to breakup – a 500 m.y.
1043 odyssey. In: Fielding, C.R., Frank, T.D., Isbell, J.L. (Eds), Resolving the Late Paleozoic Ice
1044 Age in Time and Space. Geological Society of America Special Paper 441, 1–28.
1045 Bosworth, W., Guiraud, R., Kessler, L.G., 1999. Late Cretaceous (ca. 84 Ma) compressive
1046 deformation of the stable platform of northeast Africa (Egypt): far-field stress effects of the
1047 "Santonian event" and origin of the Syrian arc deformation belt. Geology 27 (7), 633–636.
1048 Bouaziz, S., Barrier, E., Soussi, M., Turki, M.M., Zouari, H., 2002. Tectonic evolution of the
1049 northern African margin in Tunisia from paleostress data and sedimentary record.
1050 Tectonophysics 357 (1–4), 227–253. doi:10.1016/S0040-1951(02)00370-0.
1051 Boussaha, M., Thibault, N., Stemmerik, L., 2016. Integrated stratigraphy of the late
1052 Campanian–Maastrichtian in the Danish Basin: revision of the Boreal calcareous
1053 nannofossil zonation. Newsletters on Stratigraphy 49 (2), 337–360.
1054 Boussaha, M., Thibault, N., Anderskouv, K., Moreau, J., Stemmerik, L., 2017. Controls on
1055 upper Campanian–Maastrichtian chalk deposition in the eastern Danish Basin.
1056 Sedimentology, . 1998–2030. doi:10.1111/sed.12386.

1057 Boutib, L., Melki, F., Zargouni, F., 2000. Tectonique synsédimentaire d'âge Crétacé Supérieur
1058 en Tunisie Nord Orientale; blocs basculés et réorganisation des aires de subsidence. Bulletin
1059 de la Société Géologique de France 171 (4), 431–440. doi:10.2113/171.4.431.
1060 Bown, P., 1998. Calcareous Nannofossil Biostratigraphy. In: British Micropaleontology
1061 Society Publication Series. Chapman and Hall/Kluwer Academic Publishers, London, 315 p.
1062 Bown, P., Lees, J., Young, J.R., 2004. Calcareous nannoplankton evolution and diversity
1063 through time. In: Thierstein, H.R., Young, J. (Eds.), Coccolithophores, Springer, Berlin, p.
1064 481–508.
1065 Briart, A., Cornet, F.L., 1880. Note sur la carte géologique de la partie centrale de la province
1066 du Hainaut, exposée à Bruxelles. Annales de la Société Géologique de Belgique 7, B:
1067 CXLV–CXLVI.
1068 Burollet, P.F., 1956. Contribution à l'étude stratigraphique de la Tunisie centrale. Annales des
1069 Mines et de la géologie, 18. Royaume de Tunis, Ministère des Travaux Publics, Service des
1070 Mines, de l'Industrie et de l'Energie, Tunis, 352 pp.
1071 Burnett, J., 1998. Upper Cretaceous. In: Bown, P. (Ed.), Calcareous Nannofossil
1072 Biostratigraphy, British Micropaleontology Society Publication Series. Chapman and
1073 Hall/Kluwer Academic Publishers, London, p. 132–199.
1074 Chamley, H., 1989. Clay Sedimentology. Springer. Berlin, 623 pp.
1075 Chamley, H., Deconinck, J-F., Millot, G., 1990. Sur l'abondance des minéraux smectitiques
1076 dans les sédiments marins communs déposés lors des périodes de haut niveau marin du
1077 Jurassique supérieur au Paléogène. Comptes Rendus de l'Académie des Sciences Paris 311,
1078 Série II, p. 1529–1536.
1079 Channell, J.E.T., Freeman, R., Heller, F., Lowrie, W., 1982. Timing of diagenetic haematite
1080 growth in red pelagic limestones from Gubbio (Italy). Earth and Planetary Science Letters
1081 58 (2), 189–201. doi:10.1016/0012-821X(82)90193-5.

1082 Charvet, J., 1978. Etude géologique des Dinnarides de la côte dalmate au Bassin pannonique: le
1083 profil Mostar-Sarajevo-Tuzla (Yougoslavie). Thèse d'état, 554 pp.
1084 Chenot, E., Pellenard, P., Martinez, M., Deconinck, J-F., Amiotte-Suchet, P., Thibault, N.,
1085 Bruneau, L., Cocquerez, T., Laffont, R., Pucéat, E., 2016. Clay mineralogical and
1086 geochemical expressions of the "Late Campanian Event" in the Aquitaine and Paris basins
1087 (France): palaeoenvironmental implications. Palaeogeography, Palaeoclimatology,
1088 Palaeoecology 447, 42–52.
1089 Christidis, G.E., 1995. Mechanism of illitization of bentonites in the geothermal field of Milos
1090 Island Greece: evidence based on mineralogy, chemistry, particle thickness and morphology.
1091 Clays and Clay Minerals 43, 569–585.
1092 Chumakov, N.M., 2004. Climatic zones and climate of the Cretaceous period. In: Semikhatov,
1093 M.A., Chumakov, N.M. (Eds), Climate in the epochs of major biospheric transformations.
1094 Transactions of the Geological Institute of the Russian Academy of Sciences (550), 105–123
1095 (Moscow, Nauka [in Russian]).
1096 Coccioni, R., Premoli Silva, I., 2015. Revised Upper Albian–Maastrichtian planktonic
1097 foraminiferal biostratigraphy and magneto-stratigraphy of the classical Tethyan Gubbio
1098 section (Italy). Newsletters on Stratigraphy 48 (1), 47–90. doi:10.1127/nos/2015/0055.
1099 Cogné, J.-P., Humler, E., 2006. Trends and rhythms in global seafloor generation rate.
1100 Geochemistry, Geophysics, Geosystems 7 (3), 1–17.
1101 Cornet, F.L., Briart, A. 1870. Sur la division de la Craie blanche du Hainaut en quatre assises.
1102 Mémoires Couronnés et Mémoires des Savants Etrangers de l 'Académie royale de Belgique
1103 35, 26 pp., 1 pl., with 5 figs.
1104 Cramer, B.S., Toggweiler, J.R., Wright, J.D, Katz, M.E., Miller. K.G., 2009. Ocean overturning
1105 since the Late Cretaceous: inferences from a new benthic foraminiferal isotope compilation.
1106 Paleoceanography 24 (4), PA4216. doi:10.1029/2008PA001683.

1107 D'Argenio, B., Mindszenty, A., 1995. Bauxites and related paleokarst: tectonic and climatic
1108 event markers at regional unconformities. Eclogae Geologicae Helvetiae 88 (3), 453–500.
1109 Deconinck, J-F., Chamley, H., 1995. Diversity of smectite origins in the Late Cretaceous
1110 sediments: example of chalks from northern France. Clay Minerals 30 (4), 365–380.
1111 Deconinck, J-F., Amédro, F., Baudin, F., Godet, A., Pellenard, P., Robaszynski, F., Zimmerlin,
1112 I., 2005. Late Cretaceous palaeoenvironments expressed by the clay mineralogy of
1113 Cenomanian–Campanian chalks from the east of the Paris Basin. Cretaceous Research 26
1114 (2), 171–179. doi:10.1016/j.cretres.2004.10.002.
1115 Deconinck, J.F., Vanderaveroet, P., 1995. Eocene to Pleistocene clay mineral sedimentation off
1116 New Jersey, Western North Atlantic (Sites 903 and 905). *In:* Proceedings of the Ocean
1117 Drilling Program, Scientific Results 150 (eds: G.S. Mountain, K.G. Miller, P. Blum, C.W.
1118 Poag, D.C. Twichell), 147–170.
1119 Delissanti, F., Pini, G.A., Baudin, F., 2010. Use of T_{max} as a thermal maturity indicator in
1120 orogenic successions and comparison with clay mineral evolution. Clay minerlas 45, 115-
1121 130.
1122 Dera, G., Pellenard, P., Neige, P., Deconinck, J-F., Pucéat, E., Dommergues, J-L., 2009.
1123 Distribution of clay minerals in Early Jurassic Peritethyan seas: palaeoclimatic significance
1124 inferred from multiproxy comparisons. Palaeogeography, Palaeoclimatology, Palaeoecology
1125 271 (1), 39–51.
1126 Dercourt, J., Zonenshain, L.P., Ricou, L.-E., Kazmin, V.G., Le Pichon, X., Knipper, A.L.,
1127 Grandjacquet, C., Sbortshikov, I.M., Geyssant, J., Lepvrier, C., Pechersky, D.H., Boulin, J.,
1128 Sibuet, J.-C., Savostin, L.A., Sorokhtin, O., Westphal, M., Bazhenov, M.L., Lauer, J.P.,
1129 Biju-Duval, B., 1986. Geological evolution of the Tethys belt from the Atlantic to the
1130 Pamirs since the Lias. Tectonophysics 123, 241–315. doi:10.1016/0040-1951(86)90199-X.

1131 Dessert, C., Dupré, B., Gaillardet, J., François, L.M., Allègre, C.J., 2003. Basalt weathering
1132 laws and the impact of basalt weathering on the global carbon cycle. Chemical Geology 202,
1133 257–273. doi:10.1016/j.chemgeo.2002.10.001.
1134 Dewey, J.F., Pitman, W.C., Ryan, W.B.F., Bonnin, J., 1973. Plate tectonics and the evolution
1135 of the Alpine system. Geological Society of America Bulletin 84 (10), 3137–3180.
1136 Dlala, M., 2002. Les manifestations tectono-sédimentaires d'âge Campanien–Maastrichtien en
1137 Tunisie : implications sur l'évolution géodynamique de la marge Nord-Africaine. Comptes
1138 Rendus Geoscience 334 (2), 135–140. doi:10.1016/S1631-0713(02)01719-4.
1139 Dubicka, Z., Jurkowska, A., Thibault, N., Javad Razmjooei, M., Wójcike, K., Gorzelak, P.,
1140 Felisiak, I., 2017. An integrated stratigraphic study across the Santonian/Campanian
1141 boundary at Bocieniec, southern Poland: A new boundary stratotype candidate. Cretaceous
1142 Research 80, 61–85. doi: 10.1016/j.cretres.2017.07.012.
1143 Faccenna, C., Becker, T.W., Lucente, F.P., Jolivet, L., Rossetti, F., 2001. History of subduction
1144 and back arc extension in the Central Mediterranean. Geophysical Journal International 145,
1145 809–820. doi:10.1046/j.0956-540x.2001.01435.x.
1146 Franks, P.J., Royer, D.L., Beerling, D.J., Van de Water, P.K., Cantrill, D.J., Barbour, M.M.,
1147 Berry, J.B., 2014. New constraints on atmospheric CO_2 concentration for the Phanerozoic,
1148 Geophysical Research Letters 41, 4685-4694. doi:10. 1002/201 4GL060457.
1149 Friedrich, O., Herrle, P.A., Wilson, M.J., Cooper, J., Erbacher, J., Hemleben, C., 2009. Early
1150 Maastrichtian carbon cycle perturbation and cooling event: Implications from the South
1151 Atlantic Ocean. Paleoceanography 24.
1152 Friedrich, O., Norris, R.D., Erbacher, J., 2012. Evolution of middle to late Cretaceous oceans –
1153 A 55 my record of Earth's temperature and carbon cycle. Geology 40 (2), 107–110.

1154 Frizon de Lamotte, D., Leturmy, P., Missenard, Y., Khomsi, S., Ruiz, G., Saddiqi, O.,
1155 Guillocheau, F., Michard, A., 2009. Mesozoic and Cenozoic vertical movements in the Atlas
1156 system (Algeria, Morocco, Tunisia): an overview. Tectonophysics 475, 9–28.
1157 Frizon de Lamotte, D., Raulin, C., Mouchot, N., Wrobel-Daveau, J-C., Blanpied, C.,
1158 Ringenbach, J-C., 2011. The southernmost margin of the Tethys realm during the Mesozoic
1159 and Cenozoic: initial geometry and timing of the inversion processes. Tectonics 30 (3),
1160 TC3002. doi:10.1029/2010TC002691.
1161 Gale, A.S., Hancock, J.M., Kennedy, W.J., Petrizzo, M.R., Lees, J.A., Walaszczyk, I., Wray,
1162 D.S., 2008. An integrated study (geochemistry, stable oxygen and carbon isotopes,
1163 nannofossils, planktonic foraminifera, inoceramid bivalves, ammonites and crinoids) of the
1164 Waxahachie Dam spillway section, North Texas: a possible boundary stratotype for the base
1165 of the Campanian Stage. Cretaceous Research 29 (1), 131–167.
1166 doi:10.1016/j.cretres.2007.04.006.
1167 Gale, A., Anderskouv, K., Surlyk, F., Whalley, J., 2015. Slope failure of chalk channel
1168 margins: implications of an Upper Cretaceous mass transport complex, southern England.
1169 Journal of the Geological Society 172, 763–776.
1170 Gibbs, 1977. Clay mineral segregation in the marine environment. Journal of Sedimentary
1171 Research 47, 237–243.
1172 Goddéris, Y., François, L.M., 1995. The Cenozoic evolution of the strontium and carbon
1173 cycles: relative importance of continental erosion and mantle exchanges. Chemical Geology
1174 126, 169–190.
1175 Guiraud, R., Bosworth, W., 1999. Phanerozoic geodynamic evolution of northeastern Africa
1176 and the northwestern Arabian platform. Tectonophysics 315 (1–4), 73–104.
1177 Haq, B.U., Hardenbold, J., Vail., P.R., 1988. Mesozoic and Cenozoic chronostratigraphy and
1178 cycles of sea-level change. In: Wilgus, C.K., Hasting, B.S., C.S., Posamentier, H.W., Ross,

C.A., Van Wagoner, J.C. (eds) Sea-Level Changes: An Integrated Approach, SEPM, Tulsa, Special Publication, 42, 71–108.

Haq, B.U. 2014. Cretaceous eustasy revisited. Global and Planetary Change, 113, 44–58. doi: 10.1016/j.gloplacha.2013.12.007.

Hardenbold, J., Thierry, J., Farley, M.B., Jacquin, T., De Graciansky, P.-C., Vail, P.R., 1998. Mesozoic and Cenozoic sequance chronostratigraphic framework of European basin. In: De Graciansky, P.C., Hardenbold, J., Jacquin, T., Vail, P.R. (eds) Mesozoic and Cenozoic Sequence Stratigraphy of European Basins. SEPM Special Publications, 60, chart 5.

Hardman, R.F.P., 1982. Chalk reservoirs of the North Sea. Bulletin of the Geological Society of Denmark 30, 119–137.

Hermoso, M., Pellenard, P., 2014. Continental weathering and climatic changes inferred from clay mineralogy and paired carbon isotopes across the early to middle Toarcian in the Paris Basin. Palaeogeography, Palaeoclimatology, Palaeoecology 399, 385–393.

Huber, B.T., Hodell, D.A., Hamilton, C.P., 1995. Middle–Late Cretaceous climate of the southern high latitudes: stable isotopic evidence for minimal equator-to-pole thermal gradients. Geological Society of America Bulletin 107, 1164–1191.

Inoue, A., Bouchet, A., Velde, B., Meunier, A., 1989. Convenient technique for estimating smectite layer percentage in randomly interstratified illite/smectite minerals. Clays and Clay Minerals 37, 227–234.

Jarvis, I., 2006. The Santonian–Campanian phosphatic chalks of England and France. Proceedings of the Geologists' Association, 117, 219–237.

Jarvis, I., Mabrouk, A., Moody, R.T.J., De Cabrera, S., 2002. Late Cretaceous (Campanian) carbon isotope events, sea-level change and correlation of the Tethyan and Boreal realms. Palaeogeography, Palaeoclimatology, Palaeoecology 188, 215–248.

1203 Jarvis, I., Gale, A.S., Jenkyns, H.C., Pearce, M.A., 2006. Secular variation in Late Cretaceous
1204 carbon isotopes: a new $\delta^{13}C$ carbonate reference curve for the Cenomanian–Campanian
1205 (99.6–70.6 Ma). Geological Magazine 143 (05), 561–608.
1206 doi:10.1017/S0016756806002421.
1207 Jeans, C.V., 2006. Clay mineralogy of the Cretaceous strata of the British Isles. Clay Minerals,
1208 41, 47-150.
1209 Jenkyns, H.C., Gale, A.S., Corfield, R.M., 1994. Carbon-and oxygen-isotope stratigraphy of the
1210 English Chalk and Italian Scaglia and its palaeoclimatic significance. Geological Magazine
1211 131 (1), 1–34.
1212 Jenkyns, H.C., Mutterlose, J., Sliter, W.V., 1995. Upper Cretaceous carbon-and oxygen-isotope
1213 stratigraphy of deep-water sediments from the north-central Pacific (Site 869, flank of
1214 Pikinni Wodejebato, Marshall Islands). Proceedings of the Ocean Drilling Program,
1215 Scientific Results 143, 105–108.
1216 Jolivet, L., Faccenna, C., Agard, P., Frizon de Lamotte, D., Menant, A., Sternai, P.,
1217 Guillocheau, F., 2016. Neo-Tethys geodynamics and mantle convection: from extension to
1218 compression in Africa and a conceptual model for obduction. Canadian Journal of Earth
1219 Sciences 53 (11), 1190–1204. doi:10.1139/cjes-2015-0118.
1220 Jones, C.E., Jenkyns, H.C., Coe, A.L., Stephen, H.P., 1994. Strontium isotopic variations in
1221 Jurassic and Cretaceous seawater. Geochimica et Cosmochimica Acta 58, 3061–3074.
1222 Jung, C., Voigt, S., Friedrich, O., 2012. High-resolution carbon-isotope stratigraphy across the
1223 Campanian–Maastrichtian boundary at Shatsky Rise (tropical Pacific). Cretaceous Research
1224 37, 177–185. doi:10.1016/j.cretres.2012.03.015.
1225 Kadri, A., El Mabrouk, E., Merzeraud, G., 2015. “Kasserine Island” boundaries variations
1226 during the Upper Cretaceous–Eocene (central Tunisia). Journal of African Earth Sciences
1227 111, 244–257. doi:10.1016/j.jafrearsci.2015.07.027.

1228 Kley, J., Voigt, T., 2008. Late Cretaceous intraplate thrusting in central Europe: Effect of
1229 Africa-Iberia-Europe convergence, not Alpine collision. Geology 36, 839–842; doi:
1230 10.1130/G24930A.
1231 Kübler, B., Jaboyedoff, M., 2000. Illite crystallinity. Comptes Rendus de l'Académie des
1232 Sciences-Series IIA-Earth and Planetary Science 331, 75–89.
1233 Kübler, B., Goy-Eggenberger, D., 2001. La cristallinité de l'illite revisitée: un bilan des
1234 connaissances acquises ces trente dernières années. Clay minerals, 36 (2).
1235 doi.org/10.1180/000985501750177898.
1236 Li, L., Keller, G., 1998. Abrupt deep-sea warming at the end of the Cretaceous. Geology 26,
1237 (11), 995–998.
1238 Linnert, C., Robinson, S.A., Lees, J.A., Bown, P.R., Pérez-Rodríguez, I., Petrizzo, M.R.,
1239 Falzoni, F., Littler, K., Arz, J.A., Russell, E.E., 2014. Evidence for global cooling in the
1240 Late Cretaceous. Nature Communications 5, 1–7. doi: 10.1038/ncomms5194.
1241 Li, X., Jenkyns, H.C., Wang, C., Hu, X., Chen, X., Wei, Y., Huang, Y., Cui, J., 2006. Upper
1242 Cretaceous carbon-and oxygen-isotope stratigraphy of hemipelagic carbonate facies from
1243 southern Tibet, China. Journal of the Geological Society 163, 375–382.
1244 Liu, K., 2009. Oxygen and carbon isotope analysis of the Mooreville Chalk and late Santonian-
1245 early Campanian sea level and sea surface temperature changes, northeastern Gulf of
1246 Mexico, U.S.A. Cretaceous Research 30 (4), 980–900. doi:10.1016/j.cretres.2009.02.008.
1247 Lowrie, W., Alvarez, W., 1977. Upper Cretaceous–Paleocene magnetic stratigraphy at Gubbio,
1248 Italy. III. Upper Cretaceous magnetic stratigraphy. Geological Society of American Bulletin
1249 88, 367–389.
1250 Lowrie, W., Heller, F., 1982. Magnetic properties of marine limestones. Reviews of
1251 Geophysics 20, 171–192.

1252 Mabrouk El Asmi, A., 2014. Geochemical, $\delta^{13}C$ and eustatic curves as means for
1253 reconstructing and characterizing deep marine carbonate stratigraphic sequences (Upper
1254 Cretaceous, Tunisia). Arabian Journal of Geosciences 8 (2), 1195–1222. doi:
1255 10.1007/s12517-013-1243-4.
1256 Madsen, H.B., Stemmerik, L., 2010. Diagenesis of flint and porcellanite in the Maastrichtian
1257 chalk at Stevns Klint, Denmark. Journal of Sedimentary Research 80, 578–588.
1258 Martin, E.E., MacLeod, K.G., Berrocoso, A.J., Bourbon, E., 2012. Water mass circulation on
1259 Demerara Rise during the Late Cretaceous based on Nd isotopes. Earth and Planetary
1260 Science Letters 327, 111–120.
1261 Mattias, P., Montanari, A., Ristori, G.C., Paris, E., 1988. Segnalazione di un livello bentonitico
1262 nella Scaglia Rossa Campaniana Cretacica presso la Gola del Furlo nell'Appennino
1263 Marchigiano (Acqualagna, Pesaro). Mineralogica et Petrographica Acta 31, 243–258.
1264 McKenzie R., Horton, B.K., Loomis, S. E., Stockli, N.J., Planavsky, N.J., Lee, C.A., 2016.
1265 Continental arc volcanism as the principal driver of icehouse-greenhouse variability, Science
1266 352, 444–447. doi:10.1126/science.aad5787.
1267 Megson, J., Tygesen, Y.T., 2005. The North Sea Chalk: an underexplored and underdeveloped
1268 play. In: Doré, A.G. & Vining , B.A. (eds), Petroleum Geology: North-West Europe and
1269 Global Perspectives. Proceedings of the 6th Petroleum Geology Conference, 159–168.
1270 Melinte-Dobrinescu, M.C., Bojar, A.V., 2010. Late Cretaceous carbon- and oxygen isotope
1271 stratigraphy, nannofossil events and paleoclimate fluctuations in the Haţeg area (SW
1272 Romania). Palaeogeography, Palaeoclimatology, Palaeoecology 293 (3–4), 295–305.
1273 doi:10.1016/j.palaeo.2009.06.020.
1274 Moiroud, M., Pucéat, E., Donnadieu, Y., Bayon, G., Guiraud, M., Voigt, S., Deconinck, J-F.,
1275 Monna, F., 2016. Evolution of neodymium isotopic signature of seawater during the Late

Cretaceous: implications for intermediate and deep circulation. Gondwana Research 36, 503–522. doi:10.1016/j.gr.2015.08.005.

Monsels, D.A., 2016. Bauxite deposits in Suriname: Geological context and resource development. Netherlands Journal of Geosciences 95 (4), 405–418. doi:10.1017/njg.2015.28.

Moore, D.M., Reynolds, R.C., 2009. X-Ray Diffraction and the Identification and Analysis of Clay Minerals, 2nd edition. (Eds.) Oxford University Press, Oxford, New York, 378 pp.

Mort, H., Jacquat, O., Adatte, T., Steinmann, P., Föllmi, K., Matera, V., Berner, Z., Stüben, D., 2007. The Cenomanian/Turonian anoxic event at the Bonarelli Level in Italy and Spain: enhanced productivity and/or better preservation? Cretaceous Research 28, 597–612. doi:10.1016/j.cretres.2006.09.003.

Mortimore, R., Pomerol, B, 1997. Upper Cretaceous tectonic phases and end Cretaceous inversion in the Chalk of the Anglo-Paris Basin. Proceedings of the Geologists' Association 108 (3), 231–255. doi:10.1016/S0016-7878(97)80031-4.

Negra, M.H., Skelton, P.W., Gili, E., Valldeperas, F.X., Argles, T., 2016. Recognition of massive Upper Cretaceous carbonate bodies as olistoliths using rudist bivalves as internal bedding indicators (Campanian Merfeg Formation, Central Tunisia). Cretaceous Research 66, 177–193. doi:10.1016/j.cretres.2016.06.003.

Neuhuber, S., Gier, S., Hohenegger, J., Wolfring, E., Spötl, C., Strauss, P., Wagreich., M., 2016. Palaeoenvironmental changes in the northwestern Tethys during the Late Campanian *Radotruncana calcarata* Zone: Implications from stable isotopes and geochemistry. Chemical Geology 420, 280-296.

O'Brien, C.L., Robinson, S.A., Pancost, R.D., Sinninghe Damsté, J.S., Schouten, S., Lunt, D.J., Alsenz, H., Bornemann, A., Bottini, C., Brassell, S.C., Farnsworth, A., Forster, A., Huber, B.T., Inglis, G.N., Jenkyns, H.C., Linnert, C., Littler, K., Markwick, P., McAnena, A.,

1301 Mutterlose, J., Naafs, B.D.A., Püttmann, W., Sluijs, A., van Helmond, N.A.G.M.,
1302 Vellekoop, J., Wagner, T., Wrobel, N.E., 2017. Cretaceous sea-surface temperature
1303 evolution: Constraints from TEX 86 and planktonic foraminiferal oxygen isotopes. Earth-
1304 Science Reviews 172, 224–247. https://doi.org/10.1016/j.earscirev.2017.07.012
1305 Oms, O., Fondevilla, V., Riera, V., Marmi, J., Vicens, E., Estrada, R., Anadón, P., Vila, B.,
1306 Galobart, A., 2016. Transitional environments of the lower Maastrichtian South-Pyrenean
1307 Basin (Catalonia, Spain): the Fumanya member tidal flat. Cretaceous Research 57, 428–442.
1308 Otto-Bliesner, B. L., Upchurch G.R.J., 1997. Vegetation-induced warming of high-latitude
1309 regions during the Late Cretaceous period. Nature 385, 804–807.
1310 Perch-Nielsen, K., 1985. Calcareous nannofossils. *In* Plankton stratigraphy (eds) Bolli, H. M.,
1311 Saunders, J.B., Perch-Nielsen, K., pp 329 – 426 (Cambridge University Presse, Cambridge).
1312 Perdiou, A., Thibault, N., Anderskouv, K., van Buchem F., Buijs, G.J.A., Bjerrum, C.J., 2016.
1313 Orbital calibration of the late Campanian carbon isotope event in the North Sea. Journal of
1314 the Geological Society of London 173, 504–517. doi:10.1144/jgs2015-120.
1315 Petschick, R., 2010. MacDiff Ver. 4.2.6. Manual Geologisch-Palaontologisches Institute
1316 Johann Wolfgang Goethe Universität Frankfurt am Main Senckenberganlage, 32–34.
1317 Philip, J., Floquet, M., 2000. Early Campanian (83 – 80.5 Ma). In: Crasquin, S. (Coord.), Atlas
1318 Peri-Tethys, Palaeogeographic maps. Explanatory notes. Commission for the Geological
1319 Map of the World (CCGM/CCMW), Paris, 145–152.
1320 Pomerol, B., Aubry, M.P., 1977. Relation between Western European chalks and opening of
1321 the North Atlantic. Journal of Sedimentary Petrology 47, 1027–1035.
1322 Premoli Silva, I., 1977. Upper Cretaceous–Paleocene magnetic stratigraphy at Gubbio, Italy. II.
1323 Biostratigraphy. Geological Society of American Bulletin 88, 367–389.

1324 Premoli Silva, I., Sliter, W.V., 1994. Cretaceous planktonic foraminiferal biostratigraphy and
1325 evolutionary trends from the Bottaccione section, Gubbio, Italy. Palaeontographia Italica 82,
1326 2–90.
1327 Pucéat, E., Lécuyer, C., Sheppard, S.M.F., Dromart, G., Reboulet, S., Grandjean, P., 2003.
1328 Thermal evolution of Cretaceous Tethyan marine waters inferred from oxygen isotope
1329 composition of fish tooth enamels. Paleoceanography 18 (2), 1–12.
1330 Raymo, M.E., Ruddiman, W.F., 1992. Tectonic forcing of late Cenozoic climate. Nature 359,
1331 117–122.
1332 Razmjooei, M.J., Thibault, N., Kani, A., Mahanipour, A., Boussaha, M., Korte, C., 2014.
1333 Coniacian–Maastrichtian calcareous nannofossil biostratigraphy and carbon-isotope
1334 stratigraphy in the Zagros Basin (Iran): consequences for the correlation of Late Cretaceous
1335 Stage Boundaries between the Tethyan and Boreal realms. Newsletters on Stratigraphy 47,
1336 183–209.
1337 Richard, J., Sizun, J-P., Machhour, L., 2005. Environmental and diagenetic records from a new
1338 reference section for the Boreal realm: the Campanian chalk of the Mons Basin (Belgium).
1339 Sedimentary Geology 178 (1–2), 99–111. doi:10.1016/j.sedgeo.2005.04.001.
1340 Robaszynski, F., Anciaux, L., 1996. Les réserves de la craie pour ciment blanc sur les
1341 propriétés CBR à Harmignies. Report of the Ciments Belges Réunis Company.
1342 Robaszynski, F., Christensen, W.K., 1989. The upper Campanian–Lower Maastrichtian chalks
1343 of the Mons basin, Belgium: a preliminary study of belemnites and foraminifera in the
1344 Harmignies and Ciply areas. Geologie en Mijnbouw 68, 391–408.
1345 Robaszynski, F., Gonzales Donoso, J.M., Linares, D., Amédro, F., Caron, M., Dupuis, C.,
1346 Dhondt, A.V., Gartner, S., 2000. Le Crétacé Supérieur de la région de Kalaat Senan, Tunisie
1347 centrale. Litho- biostratigraphie intégrée : zone d'ammonites, de foraminifères planctoniques

et de nannofossiles du Turonien Supérieur au Maastrichtien. Bulletin du Centre de recherches Elf Exploration Production. 22 (2), 359–490.

Robaszynski, F., Dhondt, A.V., Jagt, J.W.M., 2001. Cretaceous lithostratigraphic units (Belgium). Geologica Belgica 4 (1-2), 121–134.

Robinson, S.A., Murphy, D.P., Vance, D., Thomas, D.J., 2010. Formation of "Southern Component Water" in the Late Cretaceous: evidence from Nd-isotopes. Geology 38 (10), 871–874.

Royer, D.L., Pagani, M., Beerling, D.J., 2012. Geobiological constraints on Earth system sensitivity to CO2 during the Cretaceous and Cenozoic. Geobiology 10, 298–310.

Ruffell, A., McKinley, J.M., Worden, R.H., 2002. Comparison of clay mineral stratigraphy to other proxy palaeoclimate indicators in the Mesozoic of NW Europe. Philosophical Transactions of the Royal Society London: Mathematical, Physical and Engineering Sciences 360 (1793), 675–693.

Sabatino, N., Meyers, S. R., Voigt, S., Coccioni, R., Sprovieri, M., 2018. A new high-resolution carbon-isotope stratigraphy for the Campanian (Bottaccione section): Its implications for global correlation, ocean circulation, and astrochronology. Palaeogeography, Palaeoclimatology, Palaeoecology, doi.org/10.1016/j.palaeo.2017.08.026.

Schönfeld, J., Sirocko, F., Jørgensen, N. O., 1991. Oxygen isotope composition of Upper Cretaceous chalk at Lägerdorf (NW Germany): its original environmental signal and palaeotemperature interpretation. Cretaceous Research 12 (1), 27–46. doi:10.1016/0195-6671(91)90025-8.

Şengör, A.C., Stock, J., 2014. The Ayyubid orogen: an ophiolite obduction-driven orogen in the Late Cretaceous of the Neo-Tethyan south margin. Geoscience Canada 41, 225–254.

1371 Schmid, S.M., Bernoulli, D., Fügenschuh, B., Matenco, L., Schefer, S., Schuster, R., Tischler,
1372 M., Ustaszewski, K., 2008. The Alpine-Carpathian-Dinaridic orogenic system: correlation
1373 and evolution of tectonic units. Swiss Journal of Geosciences 101, 139–183.
1374 Sissingh, W., 1977. Biostratigraphy of Cretaceous calcareous nannoplankton. Geologie en
1375 Mijnbouw 56, 37–56.
1376 Smith, A.G., 1971. Alpine deformation and the oceanic areas of the Tethys, Mediterranean, and
1377 Atlantic. Geological Society of America Bulletin 82 (8), 2039–2070.
1378 Sprovieri, M., Sabatino, N., Pelosi, N., Batenburg, S.J., Coccioni, R., Iavarone, M., Mazzola,
1379 S., 2013. Late Cretaceous orbitally-paced carbon isotope stratigraphy from the Bottaccione
1380 Gorge (Italy). Palaeogeography, Palaeoclimatology, Palaeoecology 379-380, 81–94.
1381 doi:10.1016/j.palaeo.2013.04.006.
1382 Środoń, J., Clauer, N., Huff, W., Dudek, T., & Banaś, M., 2009. K-Ar dating of the Lower
1383 Palaeozoic K-bentonites from the Baltic Basin and the Baltic Shield: implications for the
1384 role of temperature and time in the illitization of smectite. Clay minerals 44 (3), 361–387.
1385 Takashima, R., Nishi, H., Yamanaka, T., Hayashi, K., Waseda, A., Obuse, A., Tomosugi, T.,
1386 Deguchi, N., Mochizuki, S., 2010. High-resolution terrestrial carbon isotope and planktic
1387 foraminiferal records of the Upper Cenomanian to the Lower Campanian in the northwest
1388 Pacific. Earth and Planetary Science Letters 289 (3–4), 570–582.
1389 doi:10.1016/j.epsl.2009.11.058.
1390 Tardy, Y, Kobilsek, B., Paquet, H., 1991. Mineralogical composition and geographic
1391 distribution of African and Brazilian periatlantic laterites. The influence of continental drift
1392 and tropical paleoclimates during the past 150 million years and implications for India and
1393 Australia. Journal of African Earth Sciences 12 (1–2), 283–295.

1394 Thibault, N., 2016. Calcareous nannofossil biostratigraphy and turnover dynamics in the late
1395 Campanian–Maastrichtian of the tropical South Atlantic. Revue de Micropaléontologie 59,
1396 57–69.
1397 Thibault, N., Harlou, R., Schovsbo, N., Schiøler, P., Minoletti, F., Galbrun, B., Lauridsen,
1398 B.W., Sheldon, E., Stemmerik, L., Surlyk, F., 2012a. Upper Campanian–Maastrichtian
1399 nannofossil biostratigraphy and high-resolution carbon-isotope stratigraphy of the Danish
1400 Basin: towards a standard $\delta^{13}C$ curve for the Boreal Realm. Cretaceous Research 33 (1),
1401 72-90. doi:10.1016/j.cretres.2011.09.001.
1402 Thibault, N., Husson, D., Harlou, R., Gardin, S., Galbrun, B., Huret, E., Minoletti F., 2012b.
1403 Astronomical calibration of Upper Campanian–Maastrichtian carbon isotope events and
1404 calcareous plankton biostratigraphy in the Indian Ocean (ODP Hole 762C): implication for
1405 the age of the Campanian–Maastrichtian boundary. Palaeogeography, Palaeoclimatology,
1406 Palaeoecology 337–338, 52–71. doi:10.1016/j.palaeo.2012.03.027.
1407 Thibault, N., Anderskouv, K., Bjerager, M., Boldreel, L.O., Jelby, M.E., Stemmerik, L., Surlyk,
1408 F., 2015. Upper Campanian–Maastrichtian chronostratigraphy of the Skaelskør-1 core,
1409 Denmark: correlation at the basinal and global scale and implications for changes in sea-
1410 surface temperatures. Lethaia 48 (4), 549–560. doi:10.1111/let.12128.
1411 Thibault, N., Harlou, R., Schovsbo, N.H., Stemmerik, L., Surlyk, F., 2016a. Late Cretaceous
1412 (Late Campanian—Maastrichtian) sea surface temperature record of the Boreal Chalk Sea.
1413 Climate of the Past, 12, 1–10. doi: 10.5194/cp-12-1-2016.
1414 Thibault, N., Jarvis, I., Voigt, S., Gale, A. S., Attree, K., Jenkyns, H. C., 2016b. Astronomical
1415 calibration and global correlation of the Santonian (Cretaceous) based on the marine carbon
1416 isotope record. Paleoceanography 31. doi:10.1002/2016PA002941.
1417 Thiry, M., 2000. Palaeoclimatic interpretation of clay minerals in marine deposits: an outlook
1418 from the continental origin. Earth-Science Reviews 49, 201–221.

1419 Thiry, M., Jacquin, T., 1993. Clay mineral distribution related to rift activity, sea-level changes
1420 and paleoceanography in the Cretaceous of the Atlantic Ocean. Clay Minerals 28, 61–84.
1421 Van Der Meer, D.G., Zeebe, R., Van Hisbergen., D.J.J., Sluijs, A., Sparkman, W., Torsvik,
1422 T.H., 2014. Plate tectonic controls on atmospheric CO_2 levels since the Triassic.
1423 Proceedings of the National Academy of Sciences USA 111, 4380–4385.
1424 doi:10.1073/pnas.1315657111, 10.1073/pnas.1315657111.
1425 Vandycke, S., Bergerat, F., 1989. Analyse microtectonique des déformations cassantes dans le
1426 Bassin de Mons. Reconstruction des paléo-champs de contrainte au Crétacé-Tertiaire.
1427 Annales de la Société Géologique de Belgique, Tome 112, Fascicule 2, 469–478.
1428 Vergés, J., Fernàndez, M., Martìnez, A., 2002. The Pyrenean orogen: pre-, syn-, and post-
1429 collisional evolution. Journal of the Virtual Explorer 08. doi:10.3809/jvirtex.2002.00058.
1430 Voigt, S., Wagreich, M., Surlyk, F., Walaszczyk, I., Uličný, D., Čech, S., Voigt, T., Wiese, F.,
1431 Wilmsen, M., Niebuhr, B., Reich, M., Funk, H., Michalík, J., Jagt, J.W.M., Felder, P.J.,
1432 Schulp, A., 2008. Cretaceous In: McCann T (Ed.) Geology of Central Europe, vol 2,
1433 Geological Society, London, 923–997.
1434 Voigt, S., Friedrich, O., Norris, R.D., Schönfeld, J., 2010. Campanian–Maastrichtian carbon
1435 isotope stratigraphy: shelf-ocean correlation between the European shelf sea and the tropical
1436 Pacific Ocean. Newsletters on Stratigraphy 44 (1), 57–72.
1437 Voigt, S., Gale, A.S., Jung, C., Jenkyns, H.C., 2012. Global correlation of Upper Campanian–
1438 Maastrichtian successions using carbon-isotope stratigraphy: development of a new
1439 Maastrichtian timescale. Newsletters on Stratigraphy 45 (1), 25–53.
1440 Wagreich, M., Hohenegger, J., Neuhuber, S., 2012. Nannofossil biostratigraphy, strontium and
1441 carbon isotope stratigraphy, cyclostratigraphy and an astronomically calibrated duration of
1442 the Late Campanian *Radotruncana calcarata* Zone. Cretaceous Research 38, 80–96.

1443 Wang, Y., Huang, C., Sun, B., Quan, C., Wu, J., Lin, Z., 2014. Paleo-CO_2 variation trends and
1444 the Cretaceous greenhouse climate. Earth-Science Reviews 129, 136–147.
1445 doi:10.1016/j.earscirev.2013.11.001.
1446 Weaver, C.E., 1989. Clays, muds, and shales. Developments in Sedimentology 44, 819 pages.
1447 Wendler, I., Willems, H., Gräfe, K.-U., Ding, L., Luo, H., 2011. Upper Cretaceous inter-
1448 hemispheric correlation between the Southern Tethys and the Boreal: chemo- and
1449 biostratigraphy and paleoclimatic reconstructions from a new section in the Tethys
1450 Himalaya, S-Tibet. Newsletters on Stratigraphy 44, 137–171.
1451 Wendler, I., 2013. A critical evaluation of carbon isotope stratigraphy and biostratigraphic
1452 implications for Late Cretaceous global correlation. Earth-Science Reviews 126, 116–146.
1453 doi:10.1016/j.earscirev.2013.08.003.
1454 Willingshofer, E., Andriessen, P., Cloetingh, S.A.P.L., Neubauer, F., 2001. Detrital fission
1455 track thermochronology of Upper Cretaceous syn-orogenic sediments in the South
1456 Carpathians (Romania): inferences on the tectonic evolution of a collisional hinterland.
1457 Basin Research 13 (4), 379–395.
1458 Wolfgring, E, Hohenegger, J., Wagreich, M., 2016. Assessing pelagic palaeoenvironments
1459 using foraminiferal assemblages – A case study from the late Campanian *Radotruncana*
1460 *calcarata* Zone (Upper Cretaceous, Austrian Alps). Palaeogeography, Palaeoclimatology,
1461 Palaeoecology 441, 467 – 492.
1462 Zakharov, Y.D., Haggart, J.W., Beard, G., Safronov, P.P., 2013. Late Cretaceous climatic
1463 trends and a positive carbon isotope excursion at the Santonian–Campanian boundary in
1464 British Columbia, northeastern Pacific. Sedimentary Geology 295, 77–92.
1465 doi:10.1016/j.sedgeo.2013.08.004.

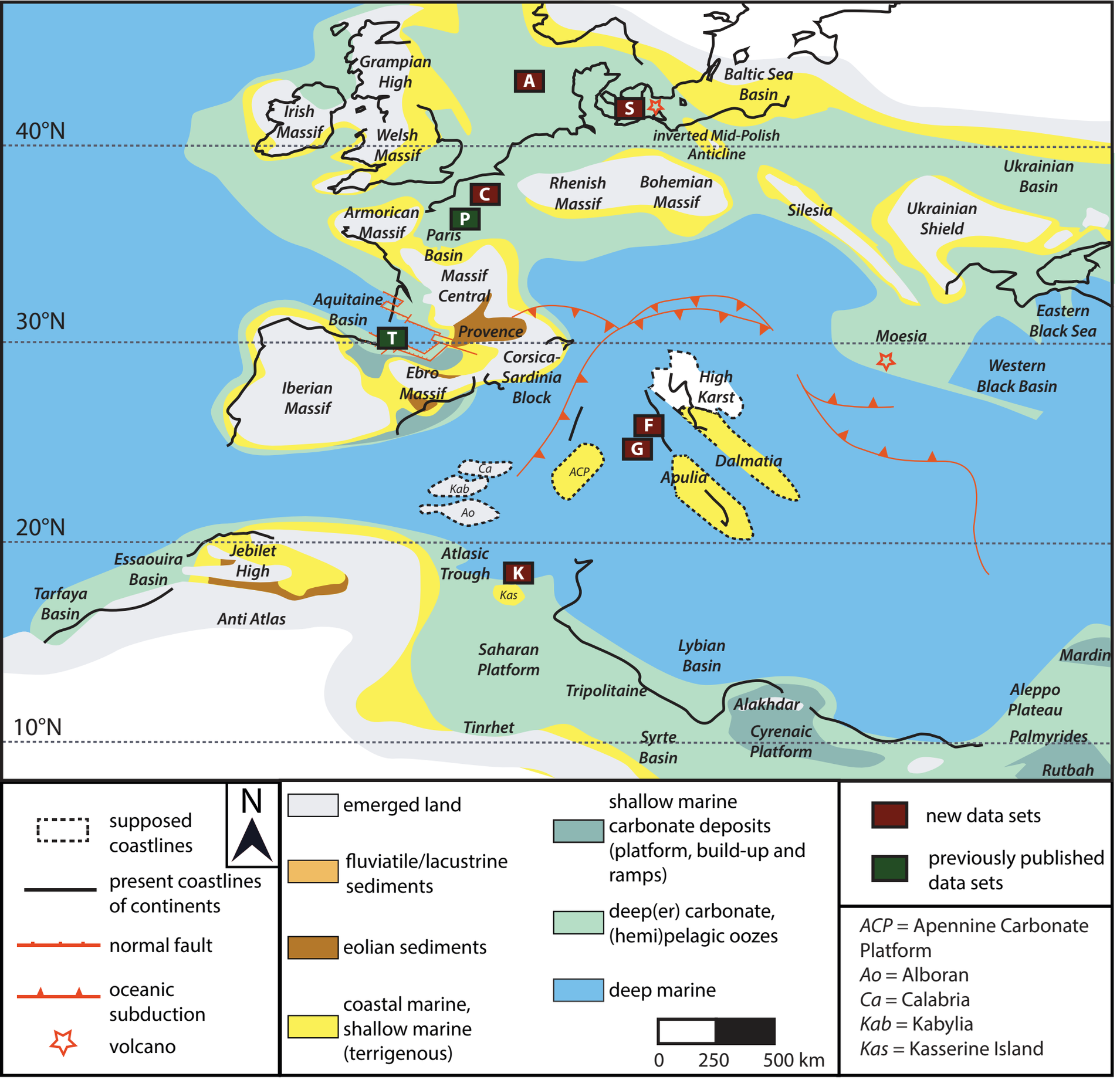
40°N
30°N
20°N
10°N
Grampian High
Irish Massif
Welsh Massif
A
S
Baltic Sea Basin
inverted Mid-Polish Anticline
Ukrainian Basin
Rhenish Massif
Bohemian Massif
Silesia
Ukrainian Shield
C
P
Armorican Massif
Paris Basin
Massif Central
Aquitaine Basin
T
Provence
Eastern Black Sea
Moesia
Western Black Basin
Corsica-Sardinia Block
Ebro Massif
Iberian Massif
High Karst
F
G
Dalmatia
Apulia
ACP
Ca
Kab
Ao
Essaouira Basin
Jebilet High
Tarfaya Basin
Anti Atlas
Atlasic Trough
K
Kas
Saharan Platform
Lybian Basin
Mardin
Tripolitaine
Aleppo Plateau
Alakhdar
Tinrhet
Syrte Basin
Cyrenaic Platform
Palmyrides
Rutbah
N
supposed coastlines
present coastlines of continents
normal fault
oceanic subduction
volcano
emerged land
fluviatile/lacustrine sediments
eolian sediments
coastal marine, shallow marine (terrigenous)
shallow marine carbonate deposits (platform, build-up and ramps)
deep(er) carbonate, (hemi)pelagic oozes
deep marine
0 250 500 km
new data sets
previously published data sets
ACP = Apennine Carbonate Platform
Ao = Alboran
Ca = Calabria
Kab = Kabylia
Kas = Kasserine Island

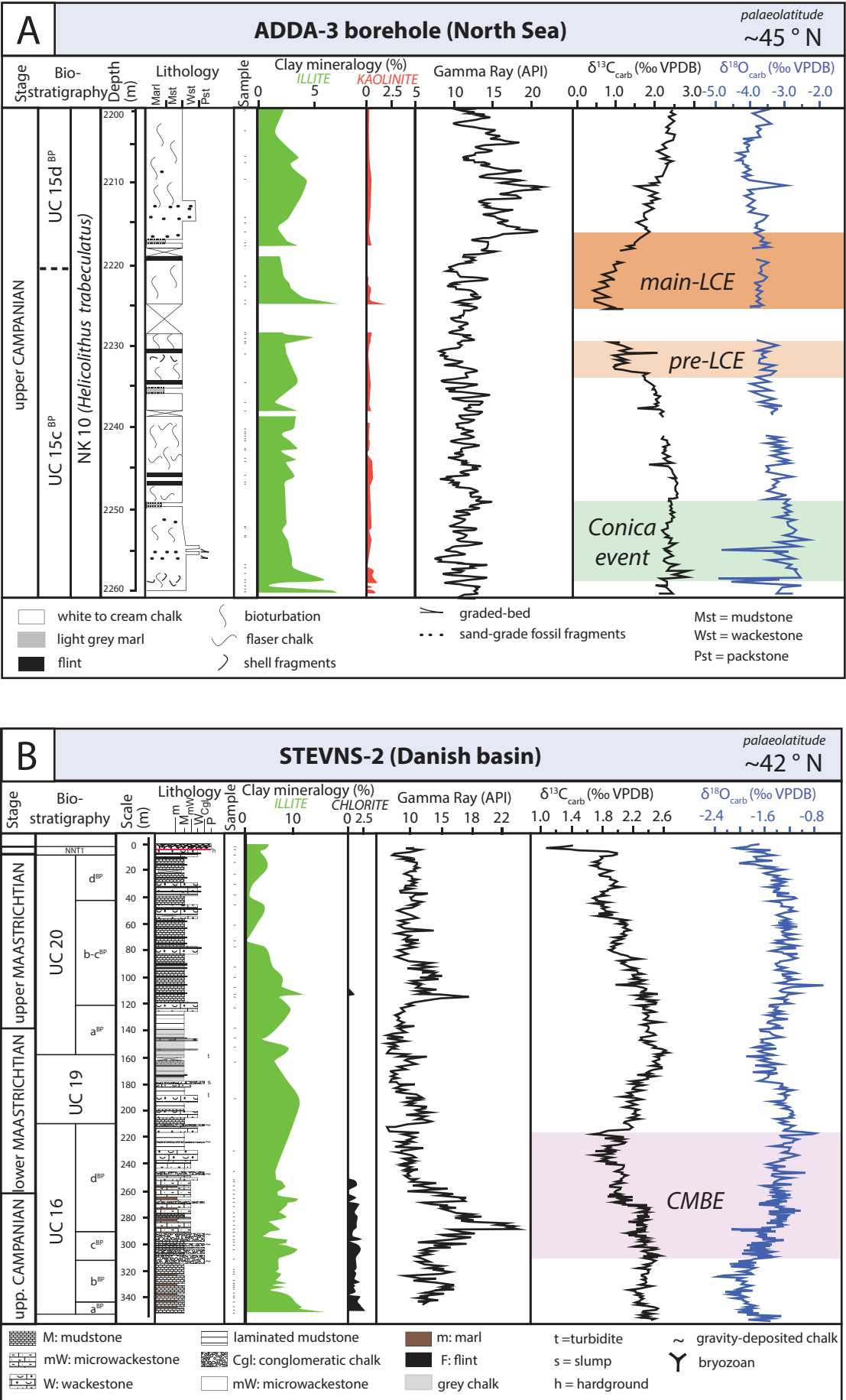
A
ADDA-3 borehole (North Sea)
palaeolatitude
~45 ° N
Stage
Bio-stratigraphy
Depth (m)
Lithology
Marl
Mst
Wst
Pst
Sample
Clay mineralogy (%)
ILLITE
KAOLINITE
Gamma Ray (API)
δ13Ccarb (‰ VPDB)
δ18Ocarb (‰ VPDB)
upper CAMPANIAN
UC 15d BP
UC 15c BP
NK 10 (Helicolithus trabeculatus)
2200
2210
2220
2230
2240
2250
2260
main-LCE
pre-LCE
Conica event
white to cream chalk
light grey marl
flint
bioturbation
flaser chalk
shell fragments
graded-bed
sand-grade fossil fragments
Mst = mudstone
Wst = wackestone
Pst = packstone
B
STEVNS-2 (Danish basin)
palaeolatitude
~42 ° N
Stage
Bio-stratigraphy
Scale (m)
Lithology
m
M
mW
W
Cgl
P
Sample
Clay mineralogy (%)
ILLITE
CHLORITE
Gamma Ray (API)
δ13Ccarb (‰ VPDB)
δ18Ocarb (‰ VPDB)
upper MAASTRICHTIAN
lower MAASTRICHTIAN
upp. CAMPANIAN
UC 20
UC 19
UC 16
NNT1
dBP
b-cBP
aBP
cBP
bBP
CMBE
M: mudstone
mW: microwackestone
W: wackestone
laminated mudstone
Cgl: conglomeratic chalk
mW: microwackestone
m: marl
F: flint
grey chalk
t =turbidite
s = slump
h = hardground
gravity-deposited chalk
bryozoan

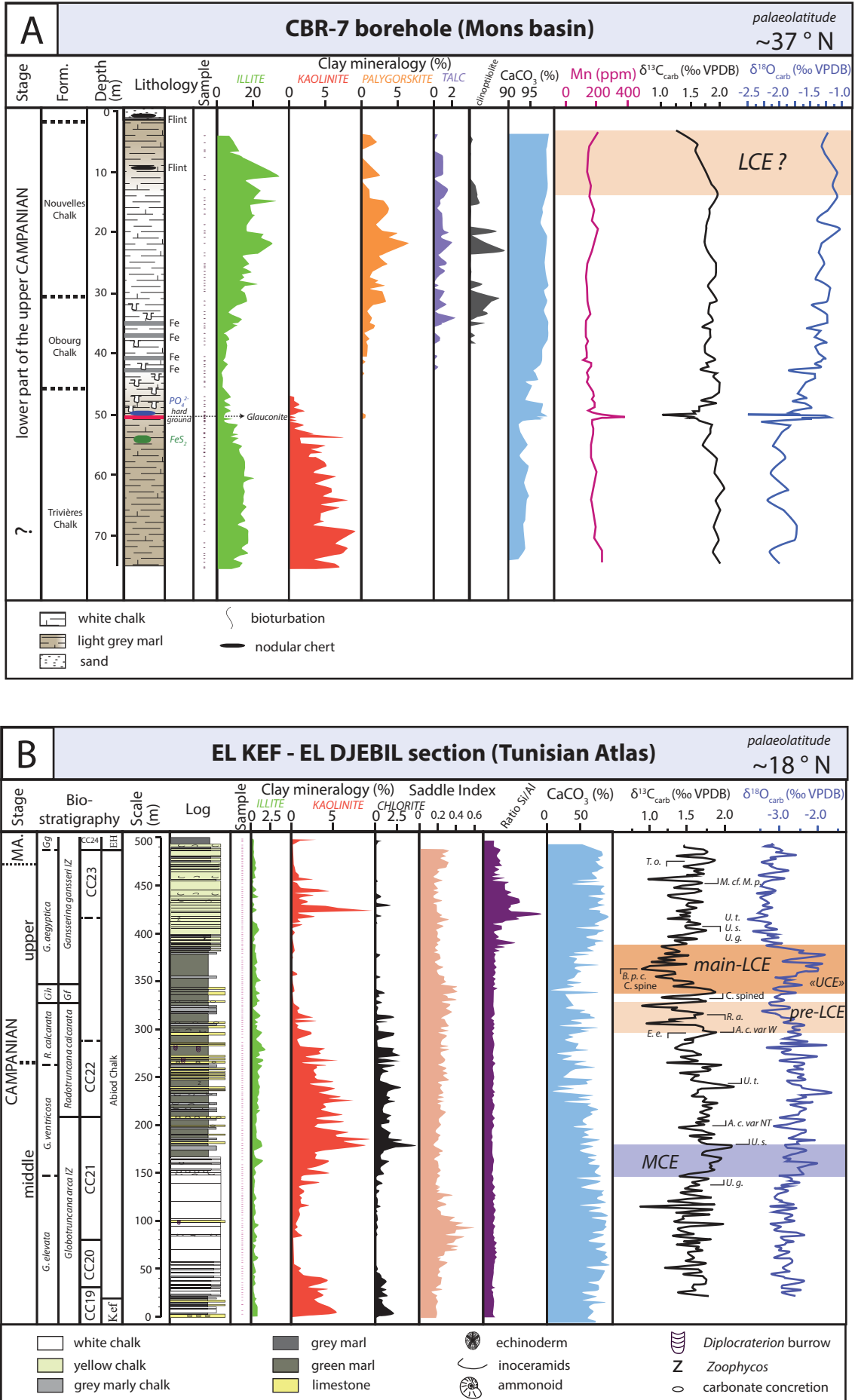
A
CBR-7 borehole (Mons basin)
palaeolatitude
~37 ° N
Stage
Form.
Depth (m)
Lithology
Sample
Clay mineralogy (%)
ILLITE
KAOLINITE
PALYGORSKITE
TALC
clinoptilolite
CaCO3 (%)
Mn (ppm)
δ13Ccarb (‰ VPDB)
δ18Ocarb (‰ VPDB)
lower part of the upper CAMPANIAN
?
Nouvelles Chalk
Obourg Chalk
Trivières Chalk
Flint
Fe
PO4 3- hard ground
Glauconite
FeS2
LCE ?
white chalk
light grey marl
sand
bioturbation
nodular chert
B
EL KEF - EL DJEBIL section (Tunisian Atlas)
palaeolatitude
~18 ° N
Stage
Bio-stratigraphy
Scale (m)
Log
Sample
Clay mineralogy (%)
ILLITE
KAOLINITE
CHLORITE
Saddle Index
Ratio Si/Al
CaCO3 (%)
δ13Ccarb (‰ VPDB)
δ18Ocarb (‰ VPDB)
MA.
upper
middle
CAMPANIAN
G. aegyptica
Gansserina gansseri IZ
R. calcarata
Radotruncana calcarata
G. ventricosa
G. elevata
Globotruncana arca IZ
CC24
CC23
CC22
CC21
CC20
CC19
EH
Abiod Chalk
Kef
T. o.
M. cf. M. p.
U. t.
U. s.
U. g.
main-LCE
B. p. c.
C. spine
«UCE»
C. spined
pre-LCE
R. a.
E. e.
A. c. var W
U. t.
A. c. var NT
U. s.
MCE
U. g.
white chalk
yellow chalk
grey marly chalk
grey marl
green marl
limestone
echinoderm
inoceramids
ammonoid
Diplocraterion burrow
Zoophycos
carbonate concretion

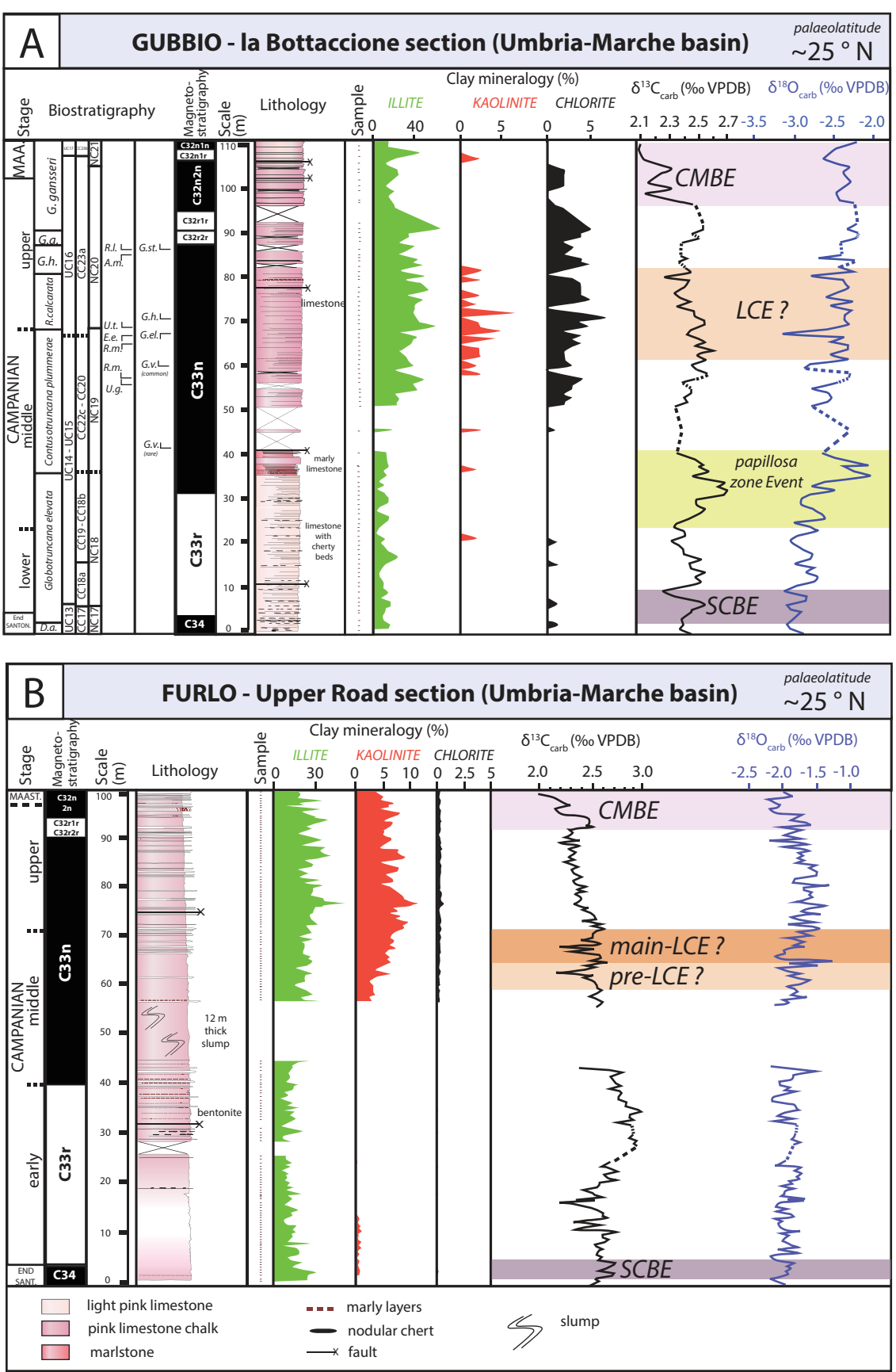
A
GUBBIO - la Bottaccione section (Umbria-Marche basin)
palaeolatitude
~25 ° N
Stage
Biostratigraphy
Magneto-stratigraphy
Scale (m)
Lithology
Sample
Clay mineralogy (%)
ILLITE
KAOLINITE
CHLORITE
δ13Ccarb (‰ VPDB)
δ18Ocarb (‰ VPDB)
MAA
upper
CAMPANIAN
middle
lower
End SANTON.
G.gansseri
G.ga.
G.h.
R.calcarata
Contusotruncana plummerae
Globotruncana elevata
D.a.
UC13
UC14 - UC15
UC16
CC18a
CC19 - CC18b
CC22c - CC20
CC23a
NC17
NC18
NC19
NC20
NC21
R.l.
A.m.
U.t.
E.e.
R.m.
U.g.
G.st.
G.el.
G.v. (common)
G.v. (rare)
C32n1n
C32n1r
C32n2n
C32r1r
C32r2r
C33n
C33r
C34
limestone
marly limestone
limestone with cherty beds
CMBE
LCE ?
papillosa zone Event
SCBE
B
FURLO - Upper Road section (Umbria-Marche basin)
palaeolatitude
~25 ° N
MAAST.
END SANT.
C32n 2n
12 m thick slump
bentonite
main-LCE ?
pre-LCE ?
light pink limestone
pink limestone chalk
marlstone
marly layers
nodular chert
fault
slump

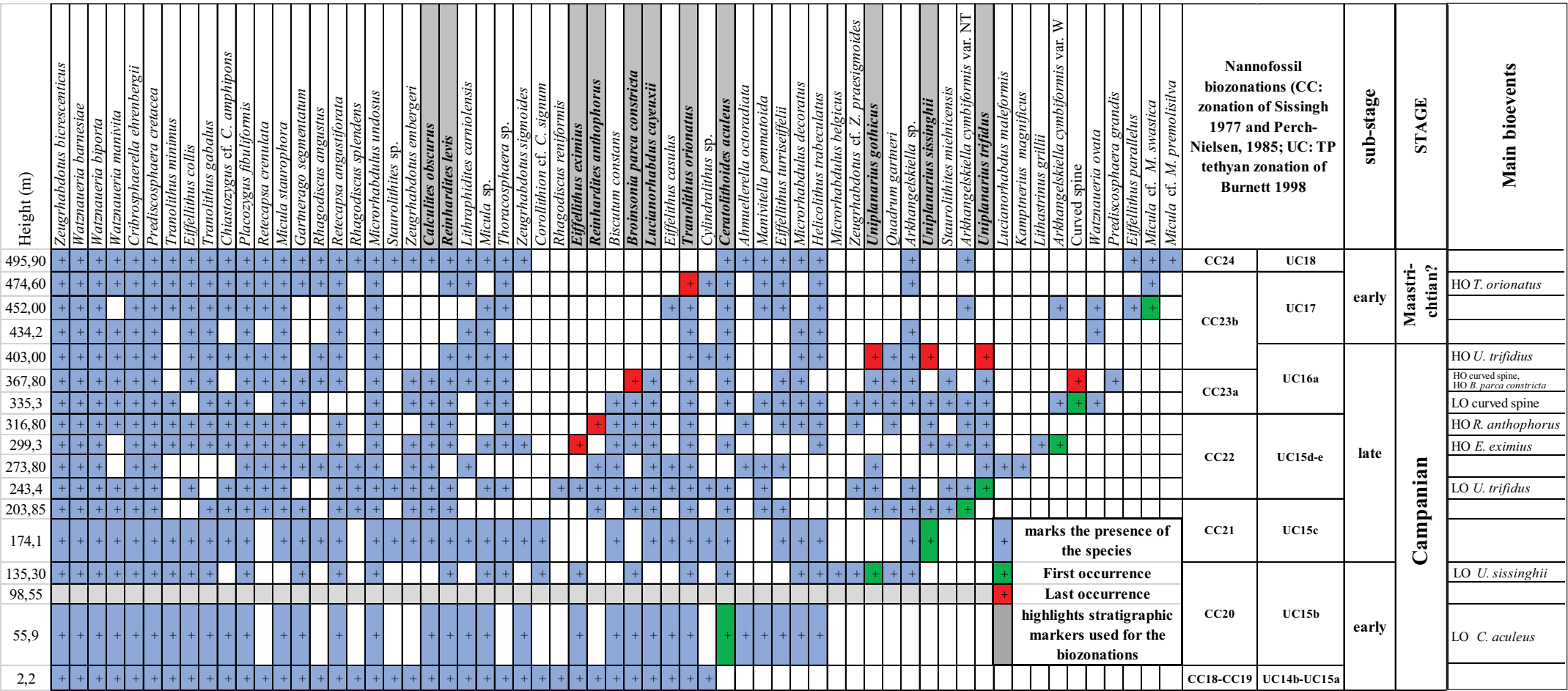
Height (m)
Zeugrhabdotus bicrescenticus
Watznaueria barnesiae
Watznaueria biporta
Watznaueria manivita
Cribrosphaerella ehrenbergii
Prediscosphaera cretacea
Tranolithus minimus
Eiffellithus collis
Tranolithus gabalus
Chiastozygus cf. C. amphipons
Placozygus fibuliformis
Retecapsa crenulata
Micula staurophora
Gartnerago segmentatum
Rhagodiscus angustus
Retecapsa angustiforata
Rhagodiscus splendens
Microrhabdulus undosus
Staurolithites sp.
Zeugrhabdotus embergeri
Calculites obscurus
Reinhardtites levis
Lithraphidites carniolensis
Micula sp.
Thoracosphaera sp.
Zeugrhabdotus sigmoides
Corollithion cf. C. signum
Rhagodiscus reniformis
Eiffellithus eximius
Reinhardtites anthophorus
Biscutum constans
Broinsonia parca constricta
Lucianorhabdus cayeuxii
Eiffellithus casulus
Tranolithus orionatus
Cylindralithus sp.
Ceratolithoides aculeus
Ahmuellerella octoradiata
Manivitella pemmatoida
Eiffellithus turriseiffelii
Microrhabdulus decoratus
Helicolithus trabeculatus
Microrhabdulus belgicus
Zeugrhabdotus cf. Z. praesigmoides
Uniplanarius gothicus
Quadrum gartneri
Arkhangelskiella sp.
Uniplanarius sissinghii
Staurolithites mielnicensis
Arkhangelskiella cymbiformis var. NT
Uniplanarius trifidus
Lucianorhabdus maleformis
Kamptnerius magnificus
Lithastrinus grilli
Arkhangelskiella cymbiformis var. W
Curved spine
Watznaueria ovata
Prediscosphaera grandis
Eiffellithus parallelus
Micula cf. M. swastica
Micula cf. M. premolisilva
Nannofossil biozonations (CC: zonation of Sissingh 1977 and Perch-Nielsen, 1985; UC: TP tethyan zonation of Burnett 1998)
sub-stage
STAGE
Main bioevents
495,90
474,60
452,00
434,2
403,00
367,80
335,3
316,80
299,3
273,80
243,4
203,85
174,1
135,30
98,55
55,9
2,2
CC24
UC18
CC23b
UC17
CC23a
UC16a
CC22
UC15d-e
CC21
UC15c
CC20
UC15b
CC18-CC19
UC14b-UC15a
early
late
early
Maastri-chtian?
Campanian
HO T. orionatus
HO U. trifidus
HO curved spine, HO B. parca constricta
LO curved spine
HO R. anthophorus
HO E. eximius
LO U. trifidus
LO U. sissinghii
LO C. aculeus
marks the presence of the species
First occurrence
Last occurrence
highlights stratigraphic markers used for the biozonations

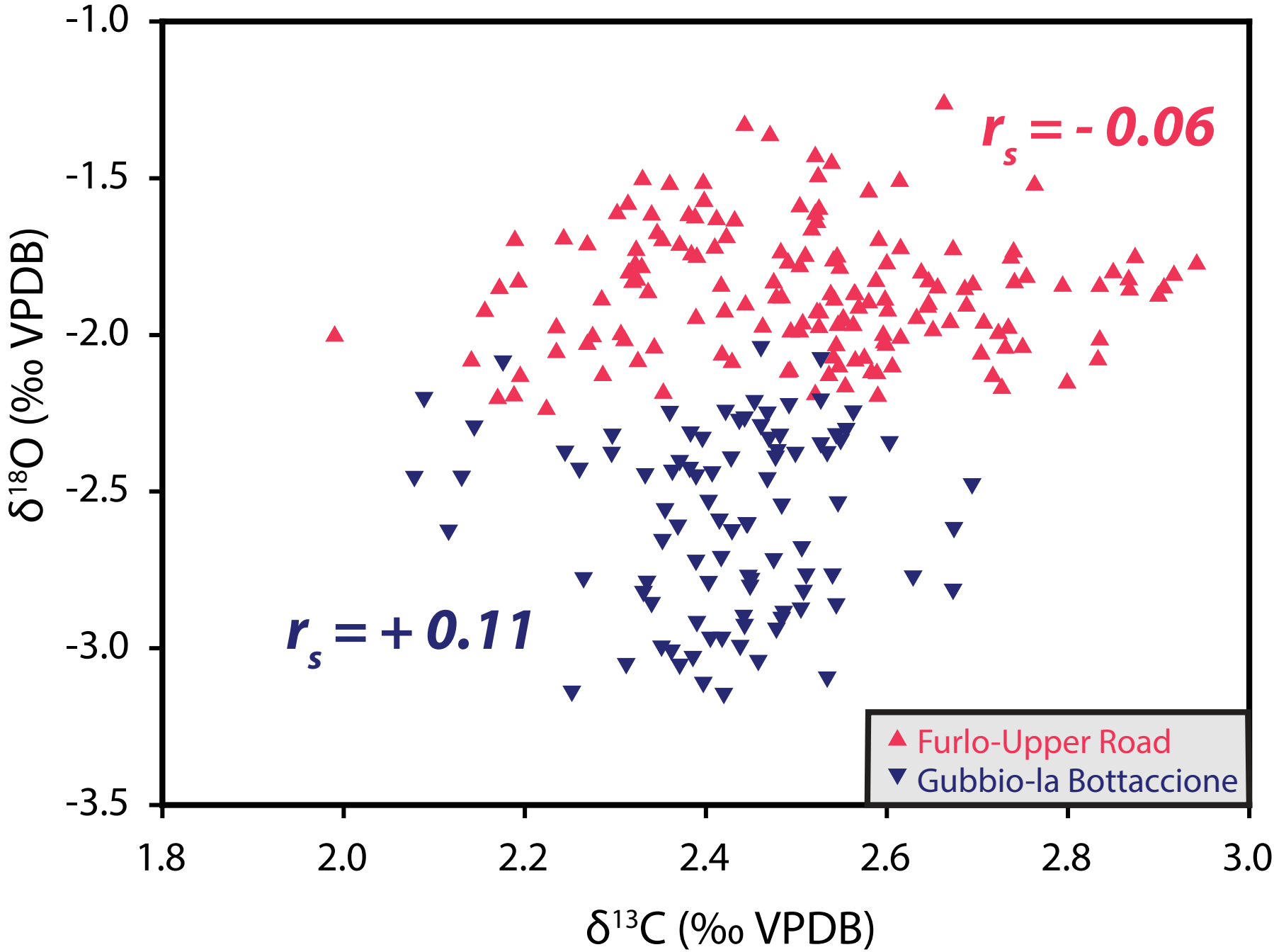
-1.0
-1.5
-2.0
-2.5
-3.0
-3.5
δ18O (‰ VPDB)
1.8
2.0
2.2
2.4
2.6
2.8
3.0
δ13C (‰ VPDB)
rs = - 0.06
rs = + 0.11
Furlo-Upper Road
Gubbio-la Bottaccione

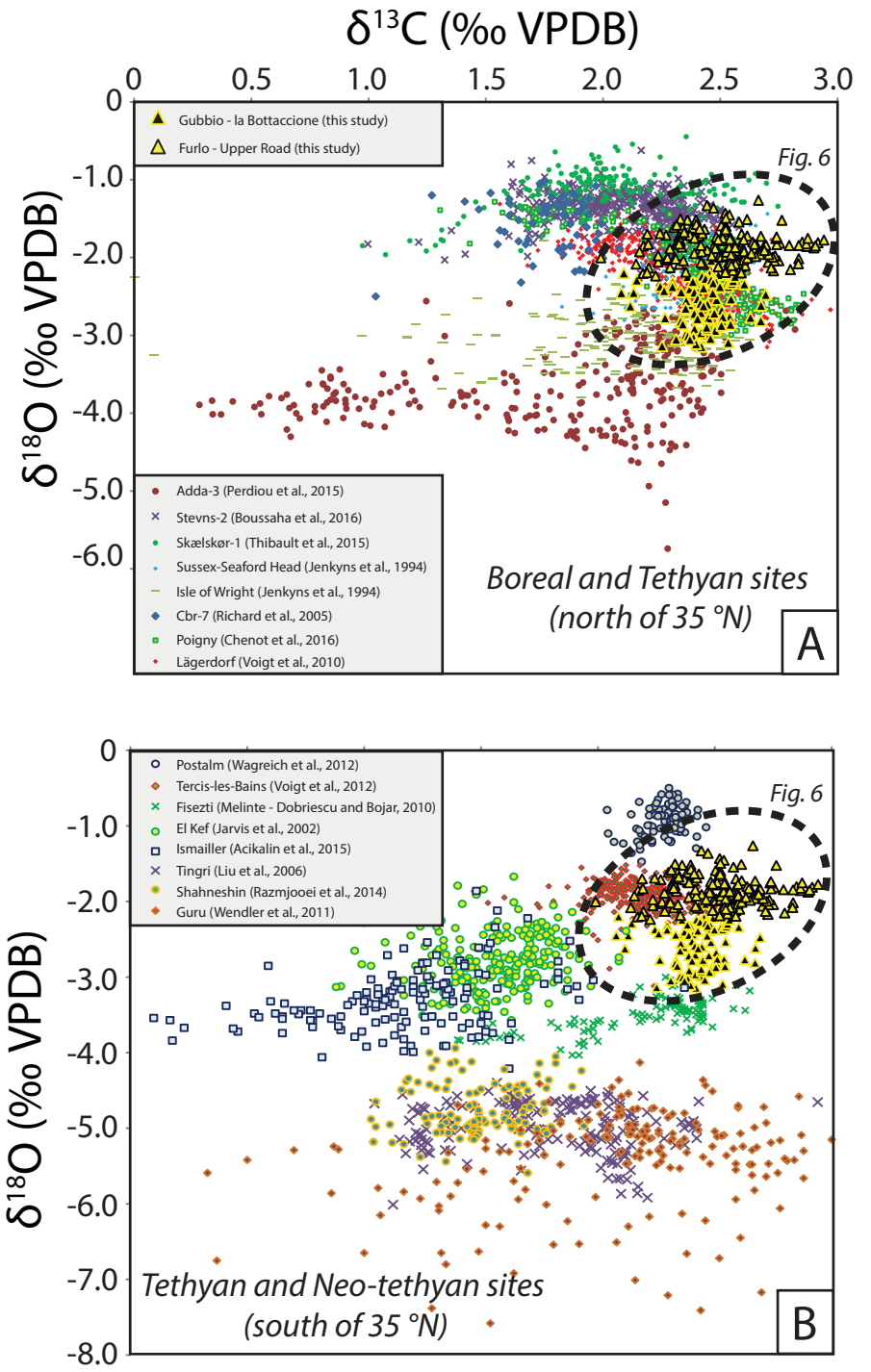
δ13C (‰ VPDB)
0
0.5
1.0
1.5
2.0
2.5
3.0
δ18O (‰ VPDB)
0
-1.0
-2.0
-3.0
-4.0
-5.0
-6.0
Gubbio - la Bottaccione (this study)
Furlo - Upper Road (this study)
Fig. 6
Adda-3 (Perdiou et al., 2015)
Stevns-2 (Boussaha et al., 2016)
Skælskør-1 (Thibault et al., 2015)
Sussex-Seaford Head (Jenkyns et al., 1994)
Isle of Wright (Jenkyns et al., 1994)
Cbr-7 (Richard et al., 2005)
Poigny (Chenot et al., 2016)
Lägerdorf (Voigt et al., 2010)
Boreal and Tethyan sites
(north of 35 °N)
A
δ18O (‰ VPDB)
0
-1.0
-2.0
-3.0
-4.0
-5.0
-6.0
-7.0
-8.0
Postalm (Wagreich et al., 2012)
Tercis-les-Bains (Voigt et al., 2012)
Fisezti (Melinte - Dobriescu and Bojar, 2010)
El Kef (Jarvis et al., 2002)
Ismailler (Acikalin et al., 2015)
Tingri (Liu et al., 2006)
Shahneshin (Razmjooei et al., 2014)
Guru (Wendler et al., 2011)
Fig. 6
Tethyan and Neo-tethyan sites
(south of 35 °N)
B

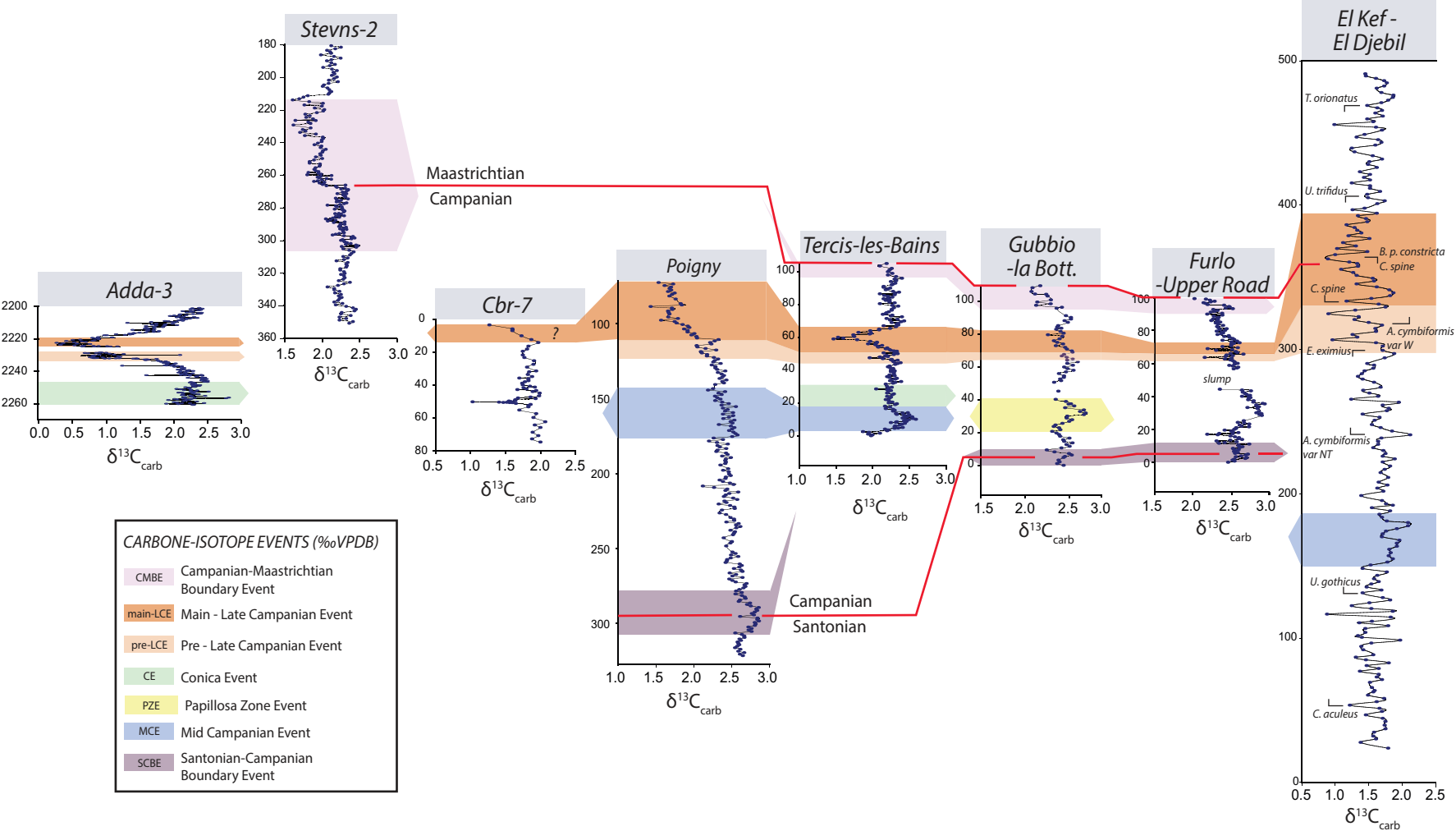

palaeo latitude	North Sea	Danish Basin	Mons Basin	Paris Basin	Aquitaine Basin	Umbria-Marche Basin	Tunisian Atlas
	~45°N	~42°N	~37°N	~36°N	~30°N	~25°N	~18°N

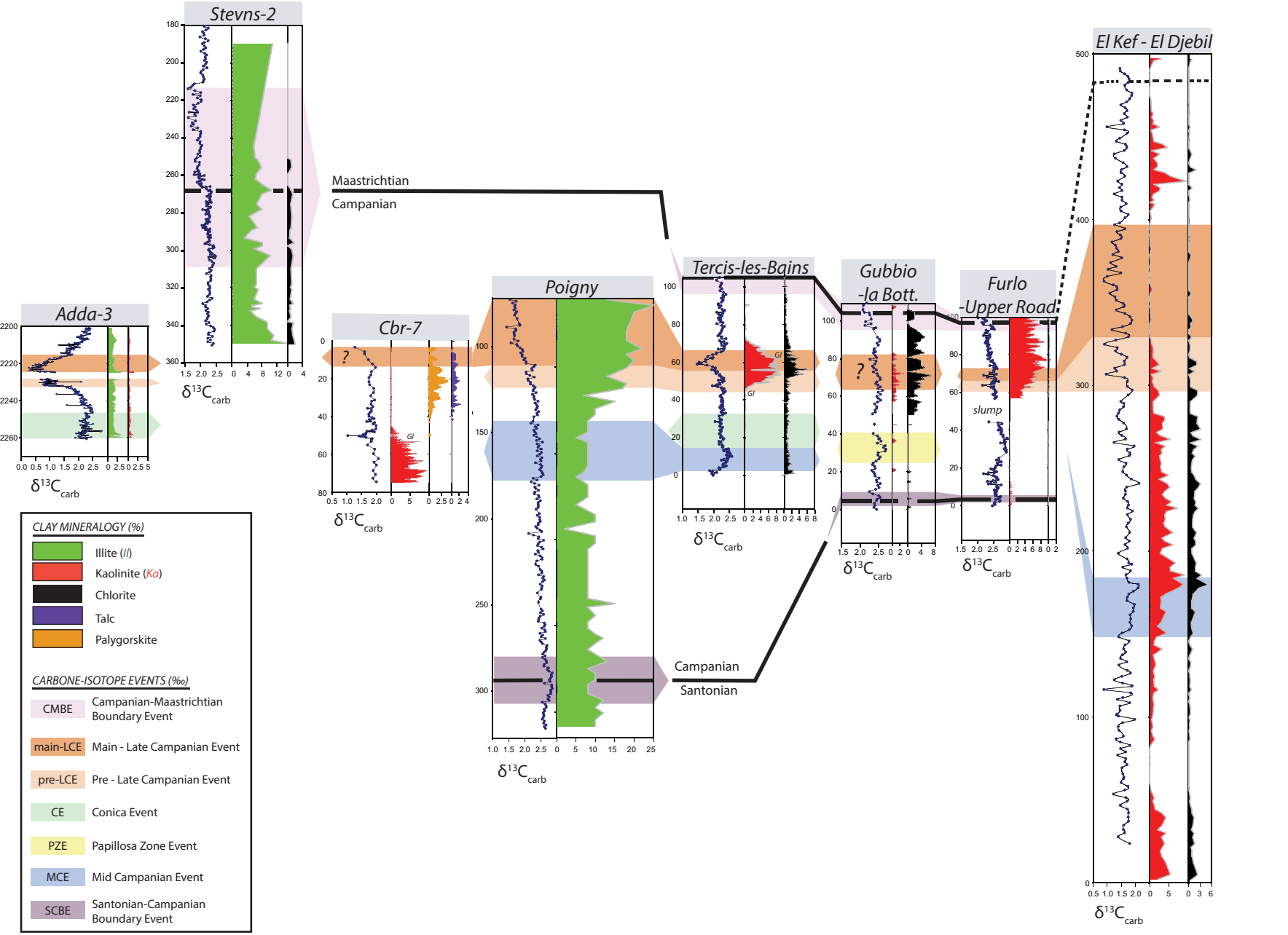
Adda-3
Stevns-2
Cbr-7
Poigny
Tercis-les-Bains
Gubbio -la Bott.
Furlo -Upper Road
El Kef - El Djebil
Maastrichtian
Campanian
Campanian
Santonian
slump
δ13Ccarb
CLAY MINERALOGY (%)
Illite (Il)
Kaolinite (Ka)
Chlorite
Talc
Palygorskite
CARBONE-ISOTOPE EVENTS (‰)
CMBE Campanian-Maastrichtian Boundary Event
main-LCE Main - Late Campanian Event
pre-LCE Pre - Late Campanian Event
CE Conica Event
PZE Papillosa Zone Event
MCE Mid Campanian Event
SCBE Santonian-Campanian Boundary Event
North Sea ~45°N
Danish Basin ~42°N
Mons Basin ~37°N
Paris Basin ~36°N
Aquitaine Basin ~30°N
Umbria-Marche Basin ~25°N
Tunisian Atlas ~18°N
palaeo latitude

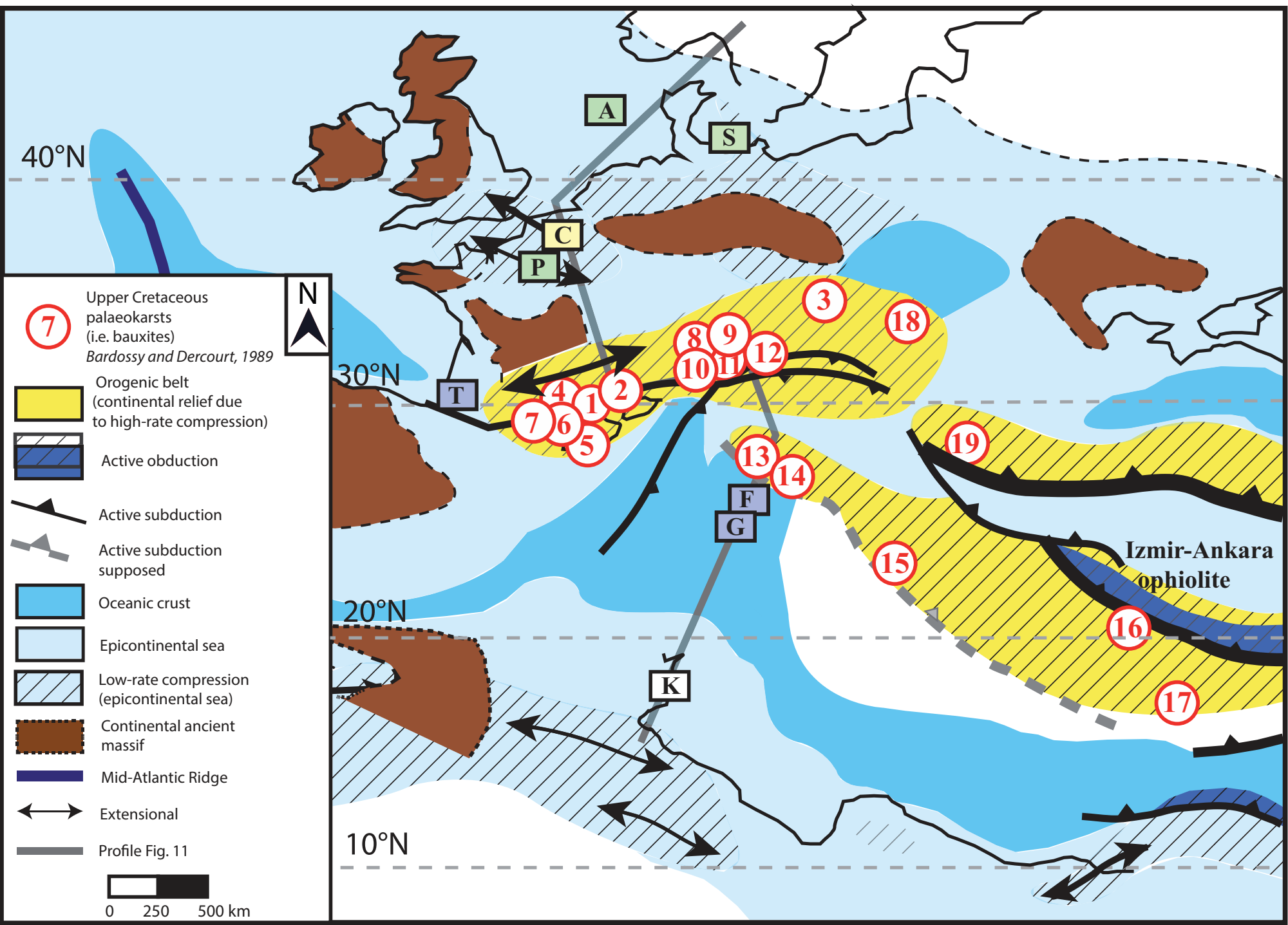
40°N
30°N
20°N
10°N
A
S
C
P
T
F
G
K
N
7
Upper Cretaceous palaeokarsts (i.e. bauxites)
Bardossy and Dercourt, 1989
Orogenic belt (continental relief due to high-rate compression)
Active obduction
Active subduction
Active subduction supposed
Oceanic crust
Epicontinental sea
Low-rate compression (epicontinental sea)
Continental ancient massif
Mid-Atlantic Ridge
Extensional
Profile Fig. 11
0 250 500 km
1
2
3
4
5
6
7
8
9
10
11
12
13
14
15
16
17
18
19
Izmir-Ankara ophiolite

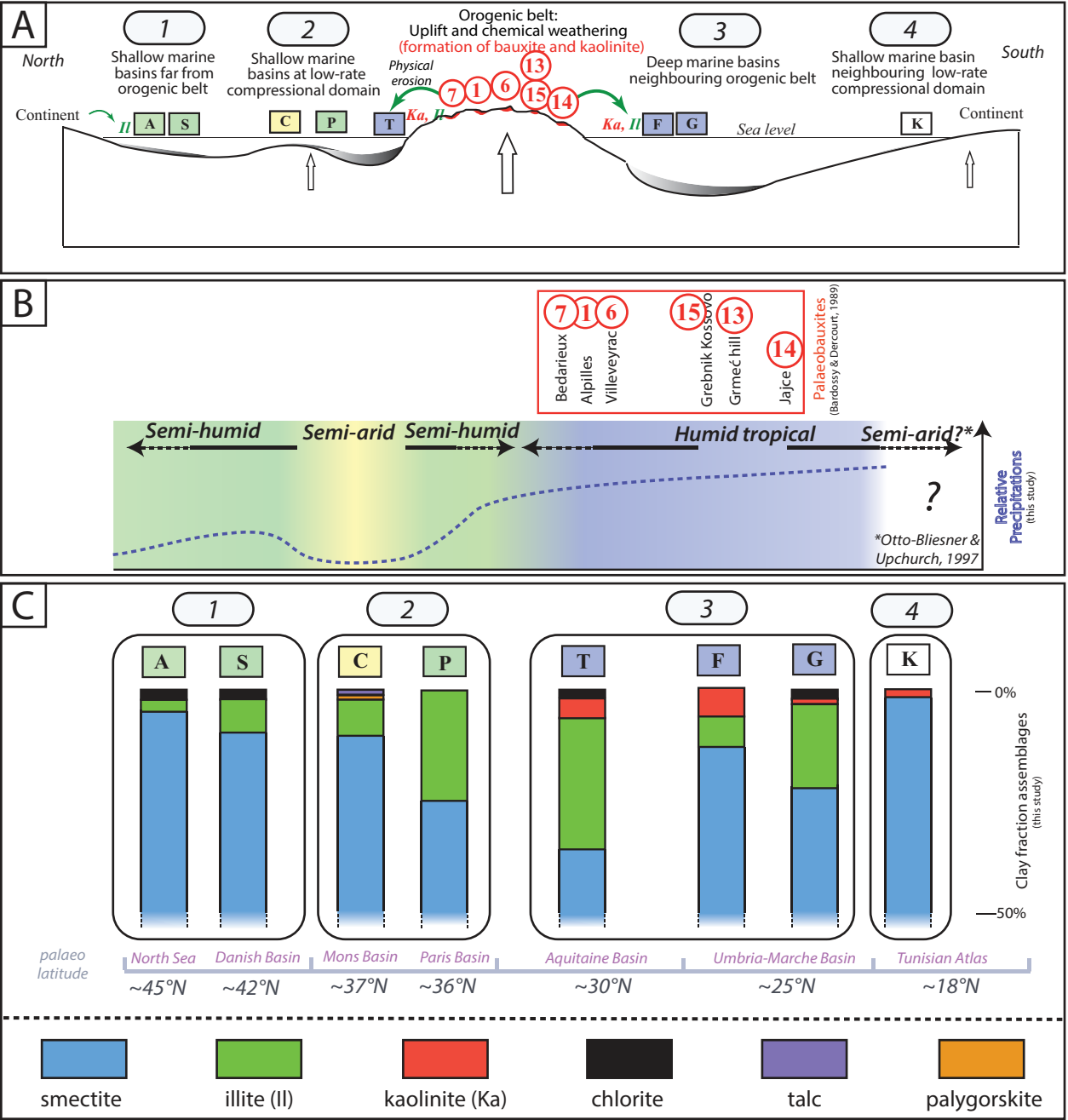
A
1
Shallow marine basins far from orogenic belt
2
Shallow marine basins at low-rate compressional domain
Orogenic belt:
Uplift and chemical weathering
(formation of bauxite and kaolinite)
Physical erosion
3
Deep marine basins neighbouring orogenic belt
4
Shallow marine basin neighbouring low-rate compressional domain
North
South
Continent
Continent
Ka, Il
Ka, Il
Sea level
B
Bedarieux
Alpilles
Villeveyrac
Grebnik Kosovo
Grmeć hill
Jajce
Palaeobauxites
(Bardossy & Dercourt, 1989)
Semi-humid
Semi-arid
Semi-humid
Humid tropical
Semi-arid?*
?
*Otto-Bliesner & Upchurch, 1997
Relative Precipitations
(this study)
C
1
2
3
4
A
S
C
P
T
F
G
K
0%
50%
Clay fraction assemblages
(this study)
palaeo latitude
North Sea
Danish Basin
Mons Basin
Paris Basin
Aquitaine Basin
Umbria-Marche Basin
Tunisian Atlas
~45°N
~42°N
~37°N
~36°N
~30°N
~25°N
~18°N
smectite
illite (Il)
kaolinite (Ka)
chlorite
talc
palygorskite

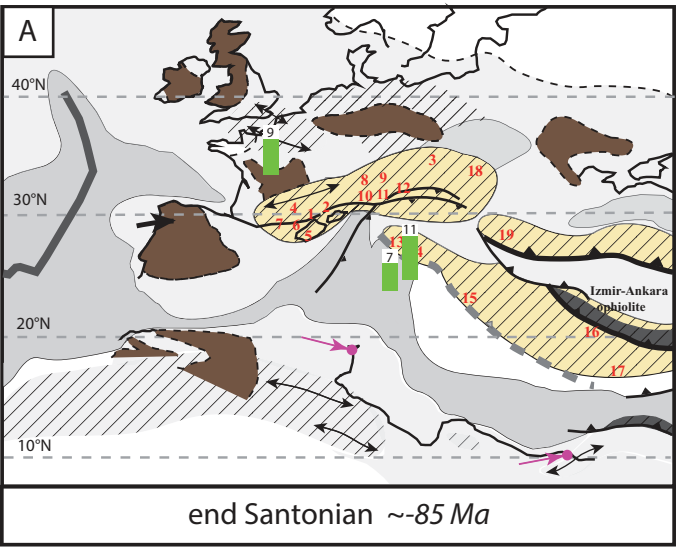

end Santonian *~-85 Ma*

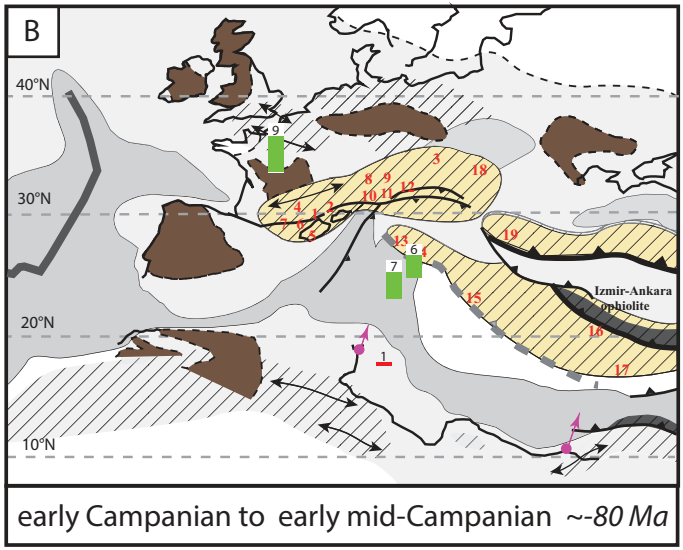

early Campanian to early mid-Campanian *~-80 Ma*

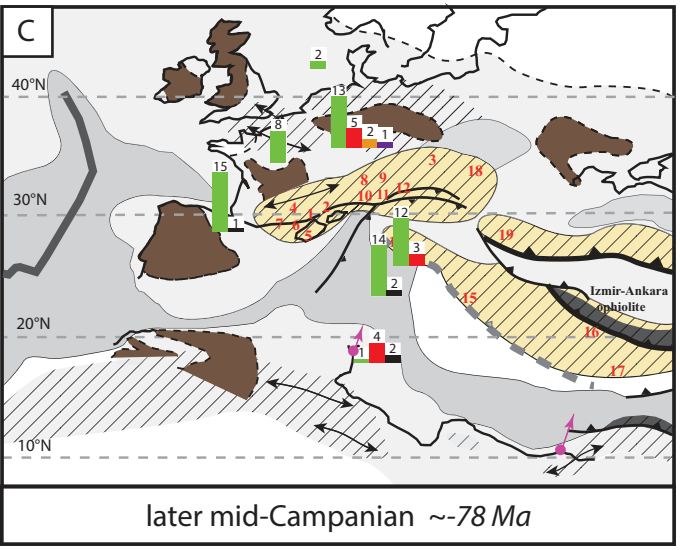

later mid-Campanian *~-78 Ma*

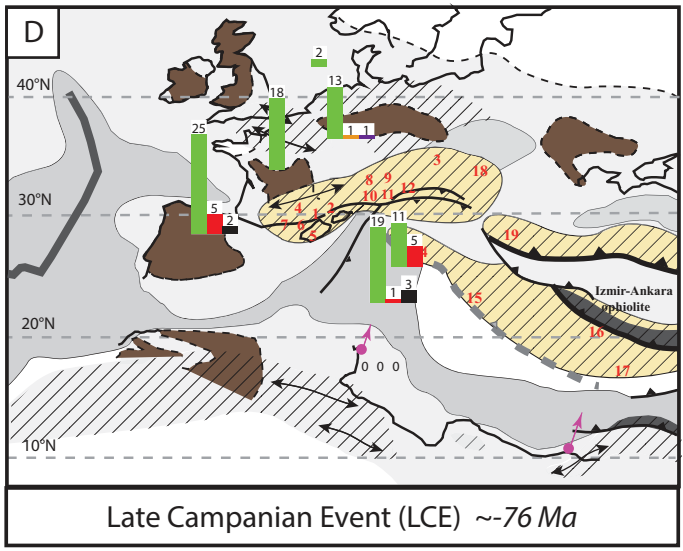

Late Campanian Event (LCE) *~-76 Ma*

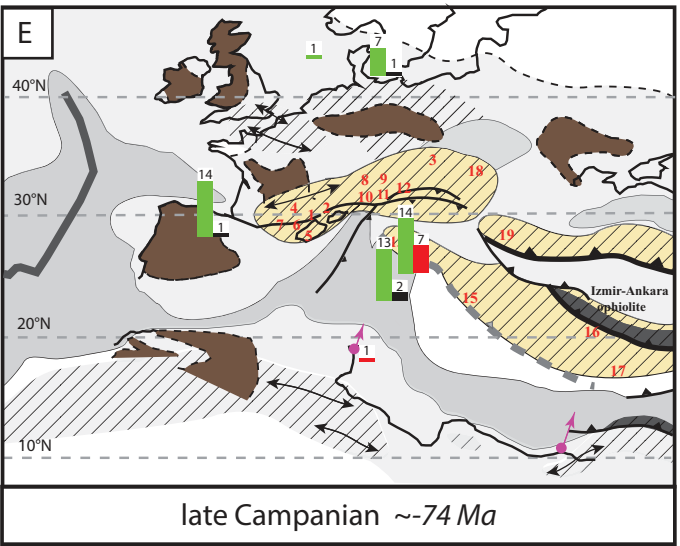

late Campanian *~-74 Ma*

7 Upper Cretaceous palaeokarsts (i.e. bauxites) *Bardossy and Dercourt, 1989*

Orogenic belt (continental relief due to high-rate compression)

Active obduction

Active subduction

Active subduction supposed

Oceanic crust

Epicontinental sea

Low-rate compression (epicontinental sea)

Continental ancient massif

Medio-atlantic Ridge

Extensional

African block direction (after *Guiraud and Bosworth, 1999*)

N

0 500 1000 km

Clay minerals (%)

illite

talc

kaolinite

palygorskite

chlorite